Journal of Computational Physics 262 (2014) 104–130

Contents lists available at ScienceDirect

Journal of Computational Physics

www.elsevier.com/locate/jcp

A procedure for the estimation of the numerical uncertainty of CFD calculations based on grid refinement studies

L. Eça [a,*], M. Hoekstra [b]

[a] Instituto Superior Técnico, Department of Mechanical Engineering, Av. Rovisco Pais, 1049-001 Lisbon, Portugal
[b] Maritime Research Institute Netherlands, PO Box 28 6700 AA, Wageningen, The Netherlands

ARTICLE INFO

Article history:
Received 22 March 2013
Received in revised form 3 January 2014
Accepted 6 January 2014
Available online 15 January 2014

Keywords:
Numerical uncertainty
Error estimation
Discretization errors

ABSTRACT

This paper offers a procedure for the estimation of the numerical uncertainty of any integral or local flow quantity as a result of a fluid flow computation; the procedure requires solutions on systematically refined grids. The error is estimated with power series expansions as a function of the typical cell size. These expansions, of which four types are used, are fitted to the data in the least-squares sense. The selection of the best error estimate is based on the standard deviation of the fits. The error estimate is converted into an uncertainty with a safety factor that depends on the observed order of grid convergence and on the standard deviation of the fit. For well-behaved data sets, i.e. monotonic convergence with the expected observed order of grid convergence and no scatter in the data, the method reduces to the well known Grid Convergence Index. Examples of application of the procedure are included.

1. Introduction

The maturing of Computational Fluid Dynamics (CFD) codes for practical calculations of complex turbulent flows comes with a need to establish the credibility of the results. Either the demands of end-users of the results or just scientific interest will sooner or later persuade or force the numerical analyst to assess the quality of his work. This quality assessment is commonly denoted as Verification & Validation.

What is to be understood by Verification & Validation in this context has been well expressed in [1]: Verification is a purely mathematical exercise that intends to show that we are "solving the equations right", whereas Validation is a science/engineering activity that intends to show that we are "solving the right equations". This means that Verification deals with numerical errors/uncertainties whereas Validation is concerned with modelling errors/uncertainties.

Verification is in fact composed of two different activities [1]: Code Verification and Solution Verification. Code Verification intends to verify, by error evaluation, that a given code solves correctly the equations of the model that it contains. On the other hand, Solution Verification intends to estimate the error/uncertainty of a given calculation, for which in general the exact solution is not known.

In the distinction between Code and Solution Verification there is mentioning of errors and uncertainties, which are conceptually different. We distinguish them, following Roache [2], as: an error requires the knowledge of the "truth/exact solution" and has a sign; an uncertainty defines an interval that should contain the "truth/exact solution" with a certain degree of confidence and is defined with a plus-minus sign.[1] Furthermore, we will estimate uncertainties as the absolute value of an error estimator multiplied by a factor of safety [2].

* Corresponding author.

[1] As stated in [3], this is not a general definition of uncertainty, but in CFD (and Engineering in general) it is widely accepted.

0021-9991/$ – see front matter
http://dx.doi.org/10.1016/j.jcp.2014.01.006

In this paper we focus on Solution Verification using systematic grid refinement, i.e. we offer a procedure for the estimation of the numerical error/uncertainty of a numerical solution for which the exact solution is unknown. Most of the existing methods for uncertainty estimation [2,4–8] require data in the so-called "asymptotic range", i.e. data on grids fine enough to give a single dominant term in a power series expansion of the error. This often means levels of grid refinement beyond those normally used in practical applications [9–11]. In order not to let this be a reason to abandon uncertainty estimation at all, we have tried to establish an uncertainty estimation procedure that accepts the practical limitations in grid density. Obviously, in the absence of contamination by round-off errors, the confidence in solutions on coarse grids will usually be less than in solutions on fine grids, which must be reflected by an increased level of uncertainty, possibly by choosing a higher factor of safety.

The present paper is organized in the following way: Section 2 presents the error estimators and the least-squares fits to estimate the error; the determination of the numerical uncertainty is described in Section 3; examples of the application of the proposed procedure are presented in Section 4 and the final remarks are summarized in Section 5. For the sake of completeness, the paper includes three appendices: the first summarizes the proposed procedure; the second presents the least-squares solution with and without weights of the (truncated) power series expansions used as error estimators and the details of the selected test cases are given in the third.

2. Error estimation

2.1. Numerical errors

It is commonly accepted [2] that the numerical error of a CFD prediction has three components: the round-off error, the iterative error and the discretization error. The round-off error is a consequence of the finite precision of the computers and its importance tends to increase with grid refinement. The iterative error is unavoidable due to the non-linearity of the mathematical equations, even if direct (non-iterative) methods can be used for the linear equations. The discretization error is a consequence of the approximations made (finite-differences, finite-volume, finite-elements,...) to transform the partial differential equations of the continuum formulation into a system of algebraic equations. Unlike the other two error sources, the relative importance of the discretization error decreases with the grid refinement.

Procedures for numerical error estimation assume the discretization error to be dominant. In practical CFD applications this is usually the case. Double-precision arithmetic makes the round-off error suitably small and in principle one should be able to reduce the iterative error to the level of the round-off error. This may not always be practically feasible though, particularly in complex flows. Nor is that strictly necessary. As suggested in [12], the iterative error should be two to three orders of magnitude smaller than the discretization error in order not to disturb the estimation of the numerical error. Anyway, in the remainder of this section, we will assume that the contribution of the round-off and iterative errors to the numerical error is negligible compared to the discretization error.

2.2. Power series representations of the discretization error

Although several types of error estimators can be found in the literature (see for example [2]), we will focus on the estimation of the discretization error with (truncated) power series expansions. The basic equation to estimate the discretization error ϵ_ϕ (see for example [1,2,5]) is:

$$\epsilon_\phi \simeq \delta_{RE} = \phi_i - \phi_o = \alpha h_i^p. \tag{1}$$

ϕ_i stands for any integral or other functional of a local flow quantity, ϕ_o is the estimate of the exact solution, α is a constant to be determined, h_i is the typical cell size and p is the observed order of grid convergence. The estimation of ϵ_ϕ requires the determination of ϕ_o, α and p. Therefore, the minimum number of grids (n_g) required for the estimation of ϵ_ϕ is three, unless p is assumed equal to a theoretical value, which is often not justified for practical problems.

The assumptions inherent in the application of Eq. (1)[2] are:

1. The grids must be in the "asymptotic range" to guarantee that the leading term of the power series expansion (high-order terms are neglected) is sufficient to estimate the error.
2. The density of the grids is representable by a single parameter, the typical cell size of the grids, h_i. This requires the grids to be geometrically similar, i.e. the grid refinement ratio must be constant in the complete field and grid properties like the deviation from orthogonality, skewness, etc. must remain unaffected.

With equal grid refinement ratios between medium/finest and coarsest/medium grids, i.e. $h_2/h_1 = h_3/h_2$, a grid triplet suffices to estimate the apparent grid convergence behaviour [1,2] based on the discriminating ratio:

$$R = \frac{\phi_1 - \phi_2}{\phi_2 - \phi_3}, \tag{2}$$

where the subscripts $_1$, $_2$ and $_3$ stand for fine, medium and coarse grid, respectively.

[2] Naturally, we are also assuming that ϕ does not include singularities, i.e. it has finite derivatives.

- Monotonic convergence for $0 < R < 1$.
- Monotonic divergence for $R > 1$.
- Oscillatory convergence for $R < 0$ and $|R| < 1$.
- Oscillatory divergence for $R < 0$ and $|R| > 1$.

In fact, the discriminating ratio R is related to the observed order of grid convergence p and the grid refinement ratios h_2/h_1 and h_3/h_2 by

$$R = \left(\frac{h_1}{h_2}\right)^p \left(\frac{(\frac{h_2}{h_1})^p - 1}{(\frac{h_3}{h_2})^p - 1}\right), \tag{3}$$

which for $h_2/h_1 = h_3/h_2$ reduces to

$$\log(R) = p\log\left(\frac{h_1}{h_2}\right). \tag{4}$$

Hence, in such conditions, $p > 0$ is equivalent to $0 < R < 1$ and $p < 0$ to $R > 1$ ($\frac{h_1}{h_2} < 1$).

Obviously, we can estimate ϵ_ϕ from Eq. (1) only when $p > 0$, the expected outcome when the three grids are in the "asymptotic range"[3] and the data have no scatter (and the code producing the data has been verified). In simple problems (simple geometry and simple equations) such requirements are easy to satisfy and Eq. (1) suffices to make a reliable error estimation. However, for what we here call "practical problems", i.e. complex geometries and complex equations (turbulent flow), it is really hard (if not impossible) to comply with all these assumptions. The consequence is that scatter appears in the data [13].

A main contributor to noisy data is the lack of geometrical similarity of the grids [14]. While structured grids essentially allow geometrical similarity to be obtained, this is hardly true for unstructured grids. Other sources of scatter in the data are flux limiters, commonly used in the discretization of convective terms, as well as damping functions and switches being part of many present-day turbulence models. Therefore, in complex flows it is an exception rather than a rule that the conditions required for the reliable use of Eq. (1) are met.

In order to be able to deal with the shortcomings of "practical calculations", we have added three other error estimators (assuming that the CFD code is theoretically second-order accurate):

$$\epsilon_\phi \simeq \delta_1 = \phi_i - \phi_o = \alpha h_i, \tag{5}$$

$$\epsilon_\phi \simeq \delta_2 = \phi_i - \phi_o = \alpha h_i^2, \tag{6}$$

and

$$\epsilon_\phi \simeq \delta_{12} = \phi_i - \phi_o = \alpha_1 h_i + \alpha_2 h_i^2. \tag{7}$$

These three alternatives are only used if the estimation with Eq. (1) is impossible or not reliable, i.e. the observed order of grid convergence is either too small or too large. The first two options ((5) and (6)) are suitable for monotonically converging solutions only whereas the latter can be used as well with non-monotonic convergence.

2.3. Least-squares error estimation

The error estimators presented above require three grids (using Eqs. (1) and (7)) or two grids (using (5) and (6)) to estimate an error. But error estimation based on three (or two) grids is not reliable for noisy data due to the extreme sensitivity of the determination of p to small perturbations in the data [13] (the use of the alternative error estimators depends on the estimated p). Therefore, it is virtually impossible to decide whether or not a given set of data is in the "asymptotic range" (in the presence of scatter, an observed order of grid convergence equal to the formal order of grid convergence may be fortuitously obtained and is not sufficient to label the data set as being in the "asymptotic range"). Furthermore, a single grid triplet gives only one instance of p, because Eq. (1) has three unknowns. Redundancy, and therefore the possibility of a quality check on the value of p, only occurs when the fourth grid is added! Therefore it is highly recommendable to use at least four grids when some scatter in the data is expected, i.e. for most engineering flow problems.

In such conditions ($n_g \geqslant 4$), it is possible to do the error estimation in the least-squares sense, i.e. to determine ϕ_o from the minimum of the functions:

[3] Usually p is equal to the theoretical order of the method, but not always [1,2].

$$S_{RE}(\phi_o,\alpha,p)=\sqrt{\sum_{i=1}^{n_g}\left(\phi_i-\left(\phi_o+\alpha h_i^p\right)\right)^2}, \tag{8}$$

$$S_1(\phi_o,\alpha)=\sqrt{\sum_{i=1}^{n_g}\left(\phi_i-\left(\phi_o+\alpha h_i\right)\right)^2}, \tag{9}$$

$$S_2(\phi_o,\alpha)=\sqrt{\sum_{i=1}^{n_g}\left(\phi_i-\left(\phi_o+\alpha h_i^2\right)\right)^2} \tag{10}$$

and

$$S_{12}(\phi_o,\alpha_1,\alpha_2)=\sqrt{\sum_{i=1}^{n_g}\left(\phi_i-\left(\phi_o+\alpha_1 h_i+\alpha_2 h_i^2\right)\right)^2}. \tag{11}$$

The least-squares minimization of Eqs. (8) to (11) is presented in Appendix B, which also includes the definition of the standard deviation of the fits σ that will be used as a measure of the quality of the fits. More information about data regressions can be found for example in [15].

2.3.1. Weighted approach

If in a practical application a flow field is computed on four (or more) grids, one may wish to give more value to the finer than the coarser grid solutions. Therefore, alternative least-squares error estimators with weights are also adopted, leading to the minimization of the following functions:

$$S_{RE}^w(\phi_o,\alpha,p)=\sqrt{\sum_{i=1}^{n_g}w_i\left(\phi_i-\left(\phi_o+\alpha h_i^p\right)\right)^2}, \tag{12}$$

$$S_1^w(\phi_o,\alpha)=\sqrt{\sum_{i=1}^{n_g}w_i\left(\phi_i-\left(\phi_o+\alpha h_i\right)\right)^2}, \tag{13}$$

$$S_2^w(\phi_o,\alpha)=\sqrt{\sum_{i=1}^{n_g}w_i\left(\phi_i-\left(\phi_o+\alpha h_i^2\right)\right)^2}, \tag{14}$$

$$S_{12}^w(\phi_o,\alpha_1,\alpha_2)=\sqrt{\sum_{i=1}^{n_g}w_i\left(\phi_i-\left(\phi_o+\alpha_1 h_i+\alpha_2 h_i^2\right)\right)^2}. \tag{15}$$

The weights w_i are based on the typical cell size:

$$w_i=\frac{\frac{1}{h_i}}{\sum_{i=1}^{n_g}\frac{1}{h_i}}, \tag{16}$$

guaranteeing that

$$\sum_{i=1}^{n_g}w_i=1. \tag{17}$$

The solution of Eqs. (12) to (15) is also given in Appendix B with the respective definition of the standard deviations of the fits, which, naturally, depend on the weights.

2.4. Proposed procedure for error estimation

Having described its main ingredients, we can now propose a procedure for the estimation of the discretization error. The procedure relies on the availability of at least four data points, on the proper choice of a typical cell size and on the assumption that the round-off and iterative errors are negligible relative to the discretization error.

The first step of the procedure is to determine the observed order of grid convergence p from the minimum of S_{RE} (Eq. (8)) and S_{RE}^w (Eq. (12)). If both solutions produce a $p>0$, we choose the best fit as the one with the smallest standard

deviation. If one of the solutions yields a negative p it is discarded. If both give negative p, the data behaviour is classified as anomalous.

Notice that we are also including oscillatory convergence as anomalous behaviour. In fact, "oscillatory convergence" is often misused to designate cases where the data in and outside the asymptotic range exhibit the opposite (slope) behaviour with grid refinement, which is better referred to as "non-monotonic convergence". We refer to oscillatory convergence when the solution is converging alternatingly above and below the exact solution. Even when more than three grids are available it is not easy to conclusively identify the convergence as oscillatory, especially when there is scatter in the data [16,17] and the scatter is comparable to the difference between solutions. We will come back to this issue at the end of this section.

2.4.1. Monotonically convergent data, $p > 0$

If the observed order of convergence is positive we proceed as follows. From what has been identified as the best fit the observed order of grid convergence p, the constant α and the estimate of the exact solution, ϕ_o, are derived. If the value of p is within an acceptable range (compared to the theoretical order of the method), the error is estimated from δ_{RE} (1). For a second-order method, the acceptable range is empirically defined here as $0.5 \leqslant p \leqslant 2$.

A value of p greater than the formal order of grid convergence (i.e. $p > 2$) is likely to cause too small error estimates. In that case, δ_{RE} is dropped and replaced by δ_1 (5) or δ_2 (6). By solving Eqs. (9), (13), (10) and (14), four fits are determined and the best fit (and the associated error estimator) is again decided from the smallest value of the standard deviation of the fit.

If on the other hand p becomes too small ($p < 0.5$), δ_{RE} produces a too conservative error estimate (when $p \to 0$, δ_{RE} tends to infinity). So for $p < 0.5$ we also drop the value of δ_{RE} in favor of the alternative error estimators with fixed exponents. In order to guarantee that we are not becoming under-conservative, we also include δ_{12} (7) in the error estimation. It means that six fits are performed in this case and the one with the smallest standard deviation is selected.

2.4.2. Anomalous data behaviour

Eq. (1) is useless for any data set that does not have $p > 0$. However, Eqs. (5), (6) and (7) may be used for any data behaviour, including non-monotonic convergence in the case of Eq. (7). Therefore, for all anomalous (non-monotonically convergent) cases the error is estimated from δ_1 (5), δ_2 (6) or δ_{12} (7) with ϕ_o, α, α_1 and α_2 determined in the least-squares sense with and without weights. As before, the selected solution is the fit involving the smallest standard deviation.

As we mentioned above, oscillatory convergence is also included in anomalous behaviour. In that case, it can be argued that we are making a very poor error estimation. However, if that is the case, this will be reflected in the value of σ and as we will describe below this will have consequences for the estimated uncertainty.

3. Uncertainty estimation

In the previous section, we described the procedure to estimate the discretization error ϵ_ϕ. The procedure gives also a measure of the quality of the error estimation, viz. the standard deviation of the fit σ, and in some cases the observed order of grid convergence p. All three quantities are used now to reach the final goal: an estimate of the uncertainty U_ϕ, i.e. an interval that contains the exact solution with 95% coverage,

$$\phi_i - U_\phi \leqslant \phi_{exact} \leqslant \phi_i + U_\phi. \tag{18}$$

First a judgement is made of the quality of the data fit. To that end we define a data range parameter as

$$\Delta_\phi = \frac{(\phi_i)_{\max} - (\phi_i)_{\min}}{n_g - 1}. \tag{19}$$

The error estimation is considered reliable if the solution is monotonically convergent with $0.5 \leqslant p < 2.1$[4] and if $\sigma < \Delta_\phi$. Following the Grid Convergence Index (GCI) procedure [1,2], the safety factor is chosen as $F_s = 1.25$ if the error estimate is deemed reliable, else $F_s = 3$.

The determination of U_ϕ, usually for the finest grid (best) solution, but essentially for any ϕ_i of a data set, is not only dependent on F_s. Different expressions are adopted for "good" and "bad" error estimations, i.e. for $\sigma \leqslant \Delta_\phi$ or $\sigma > \Delta_\phi$.

- For $\sigma < \Delta_\phi$:

$$U_\phi(\phi_i) = F_s \epsilon_\phi(\phi_i) + \sigma + |\phi_i - \phi_{fit}|. \tag{20}$$

- For $\sigma \geqslant \Delta_\phi$:

$$U_\phi(\phi_i) = 3\frac{\sigma}{\Delta_\phi}\left(\epsilon_\phi(\phi_i) + \sigma + |\phi_i - \phi_{fit}|\right). \tag{21}$$

[4] Although the error estimation does not allow $p > 2$, it is reasonable to assume a tolerance for the change in the safety factor.

The estimated uncertainty has therefore three components: the absolute value of the estimated discretization error times a safety factor; the standard deviation of the fit; the difference between the real data point and the value obtained from the fit for the same grid density. Obviously, the latter two quantities are just a consequence of scatter in the data. Consequently, for a grid refinement study with monotonically convergent smooth data the method reduces to the well-known GCI [1,2].

It could be argued that in the cases with $\sigma > \Delta_\phi$ it is not allowed to base an uncertainty estimation on the present error estimators. However, the estimated uncertainty with Eq. (21) will then be high, indicating clearly that the data quality is bad (due to e.g. grids without similarity, incomplete iterative convergence, programming mistakes in the code...), thus still conveying a useful message.

Our procedure for numerical uncertainty estimation is summarized in Appendix A.

4. Examples of application

The behaviour of the procedure presented above will now be illustrated by application to four different test cases of incompressible flow:

1. 2-D manufactured solutions that mimic a near-wall turbulent flow.
2. The turbulent flow over a flat plate.
3. The flow over a backward facing step.
4. The flow around a tanker at model scale Reynolds number.

The first test case concerns 2-D flows in a simple rectangular geometry. Because it permits the evaluation of the true discretization error, it is the ideal framework to evaluate the proposed procedure. In such conditions, we will determine the ratio between the estimated uncertainty U_ϕ and the exact error e_ϕ, $F_e = \frac{U_\phi}{e_\phi}$.

The other three test cases do not have an analytical solution. Exact errors are therefore unknown. But it is possible to check the proposed procedure by making the grid family much larger than one would normally do. This allows us to apply the procedure to subsets of grids and to verify that the results are mutually consistent, i.e. uncertainty intervals are overlapping in 95 out of 100 cases.

In the following comparisons, we will show which of the error estimations, δ_{RE} for Eq. (1), δ_1 for Eq. (5), δ_2 for Eq. (6) and δ_{12} for Eq. (7), is chosen by the procedure (without distinguishing between weighted or non-weighted fits). Such information is fundamental to demonstrate the need to consider more than the "standard" error estimator δ_{RE} in a procedure applicable to practical calculations.

In order to assess the typical difficulties of practical calculations, as for example scatter in the data and too coarse grids, we will monitor the cases with $\sigma > \Delta_\phi$, or equivalently $F_\sigma > 1$ (with $F_\sigma = \sigma/\Delta_\phi$).

Calculation details of the four test cases presented below are given in Appendix C. In the following sections, we will describe only the main features of the flow, grid sets and selected flow quantities.

4.1. 2-D manufactured solutions

The manufactured solutions (MS's) mimic a near-wall turbulent flow [18]. Three different MS's (MS1, MS2 and MS3) at a Reynolds number of $Rn = 10^7$ have been selected and they are displayed in the left part of Fig. 1. In the results presented below, we will use dimensionless variables obtained with L and U_1 as the reference length and velocity.

For each MS, we have generated three sets of 21 geometrically similar Cartesian grids in a rectangular computational domain with $0.1 \leqslant x \leqslant 1$ and $0 \leqslant y \leqslant 0.25$, where x and y are dimensionless coordinates. The finest grids include 801×801 nodes and the coarsest grids 51×51, covering a grid refinement ratio of 16. In each set, there are 4 grids between each doubling of the grid spacing, i.e. there are four groups of 6 grids that cover a grid refinement ratio of 2. The three grid sets differ only in the stretching parameter applied at $y = 0$. Grid set A has the smallest near-wall spacing and set C the largest. Next to an illustration of the three MS's, Fig. 1 presents the minimum and maximum dimensionless distance in wall coordinates[5] at the first grid node away from the wall y_2^+ for the three grid sets (the values of y_2^+ are nearly identical for the three MS's).

In this case, the grid refinement ratio is simply defined by

$$\frac{h_i}{h_1} = \frac{NX_1 - 1}{NX_i - 1} = \frac{NY_1 - 1}{NY_i - 1}, \tag{22}$$

where NX and NY are the number of grid nodes in the x and y directions, respectively.

The calculations of the three MS's were carried out with the finite-difference 2D-flow version of PARNASSOS [20] using the manufactured eddy-viscosity field. All calculations were performed with 15 digits precision and the iterative error was reduced to machine accuracy.

[5] The manufactured horizontal velocity field includes a linear sub-layer and the skin friction coefficient at $y = 0$ matches the values of an empirical correlation for turbulent flow over a flat plate.

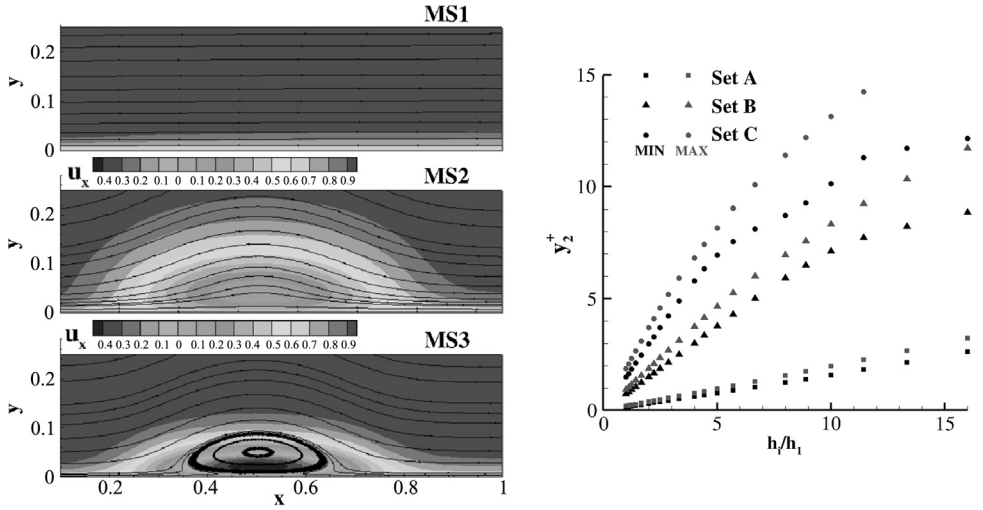

Fig. 1. Streamlines and horizontal velocity u_x isolines of the three manufactured solutions. Minimum and maximum dimensionless distance in wall coordinates at the first grid node away from the wall y_2^+ as a function of the grid refinement ratio.

Four integral quantities have been chosen to check the performance of the proposed procedure:

1. The friction resistance coefficient.

$$C_F = \frac{2}{0.9\,Rn}\int_{0.1}^{1}\left(\frac{\partial u_x}{\partial y}\right)_{y=0}\mathrm{d}x. \tag{23}$$

2. The displacement thickness at $x = 0.55$.

$$\delta^* = \int_0^{0.25}(1-u_x)\,\mathrm{d}y. \tag{24}$$

3. The momentum thickness at $x = 0.55$.

$$\theta = \int_0^{0.25}\left(u_x - u_x^2\right)\mathrm{d}y. \tag{25}$$

4. The shape factor of the horizontal velocity profile at $x = 0.55$.

$$H = \frac{\delta^*}{\theta}. \tag{26}$$

All the integrals were evaluated with a second-order trapezoidal rule.

Fig. 2 presents the results obtained for the friction resistance coefficient C_F of the MS3 (similar results are obtained for MS1 and MS2). There is a strong influence of the near-wall grid line distance on the accuracy of the C_F prediction. At least half of the data obtained in set A is in the "asymptotic range" ($p = 1.99$ for $h_i/h_1 = 1$ and $p = 1.95$ for $h_i/h_1 = 2$), whereas sets B and C may not have reached the "asymptotic range" even for the finest grids of the sets. This is an important observation because the number of grid nodes of the three sets is exactly the same. Although some of the data points are clearly outside the "asymptotic range", all estimated error bars are consistent. Logically, uncertainty estimations based on poor quality data lead to very large error bars.

Figs. 3, 4 and 5 present the convergence of δ^*, θ and H at $x = 0.55$ with the grid refinement for the MS2, which is the only MS that reveals inconsistent error bars for δ^* and θ. Both inconsistent error bars are obtained with δ_2 and a safety factor of 3 ($F_\sigma < 1$ for all the error bars estimated for the MS's). However, the two outliers occur for $h_i/h_1 = 8$ in set C, i.e. the estimated uncertainty is based on numerical solutions obtained in really coarse grids with values of y_2^+ above 8. It is interesting to remark that $H = \delta^*/\theta$ does not present an inconsistent error bar for the same data set. Nevertheless, we will discard the data obtained in the grids with $h_i/h_1 > 8$ for the check of the convergence of local flow quantities.

In each of the three grid sets, there are 361 (19×19) grid nodes common to all grids for $h_i/h_1 \leqslant 8$ (there would be 81 if we included the grids with $h_i/h_1 > 8$). Therefore, at these locations there is no need for interpolation to estimate the

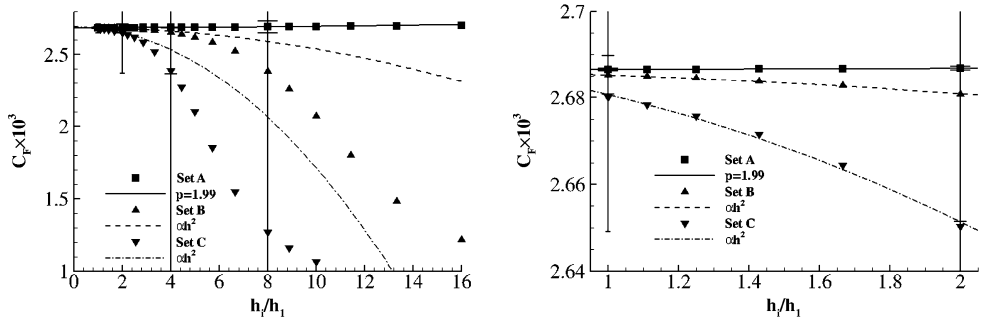

Fig. 2. Convergence of the friction resistance coefficient with the grid refinement ratio. Fits obtained from the data with $1 \leqslant h_i/h_1 \leqslant 2$. MS3 manufactured solution. (Right part of figure is detail of left part.)

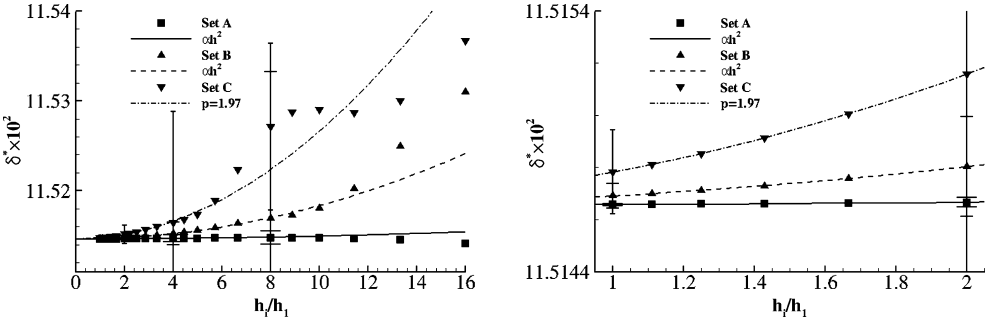

Fig. 3. Convergence of the displacement thickness δ^* at $x = 0.55$ with the grid refinement ratio. Fits obtained from the data with $1 \leqslant h_i/h_1 \leqslant 2$. MS2 manufactured solution. (Right part of figure is detail of left part.)

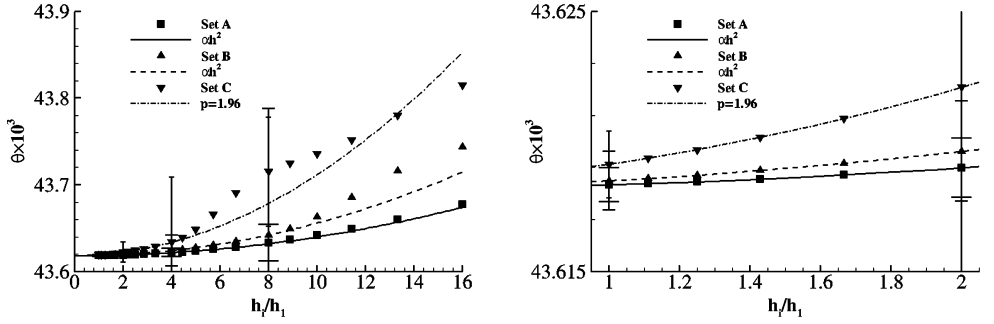

Fig. 4. Convergence of the momentum thickness θ at $x = 0.55$ with the grid refinement ratio. Fits obtained from the data with $1 \leqslant h_i/h_1 \leqslant 2$. MS2 manufactured solution. (Right part of figure is detail of left part.)

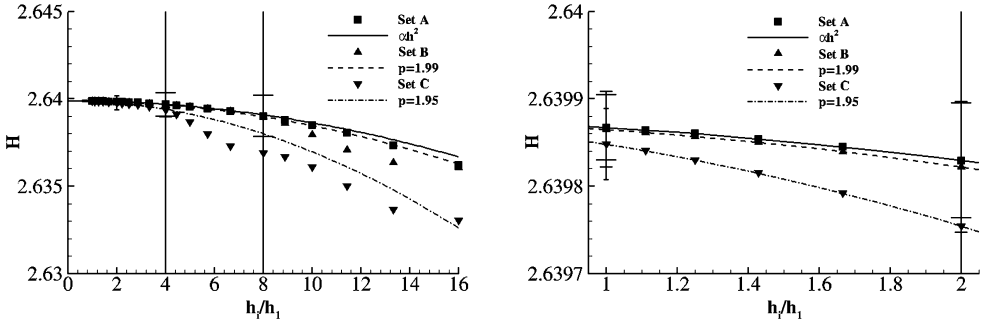

Fig. 5. Convergence of the shape factor H at $x = 0.55$ with the grid refinement ratio. Fits obtained from the data with $1 \leqslant h_i/h_1 \leqslant 2$. MS2 manufactured solution. (Right part of figure is detail of left part.)

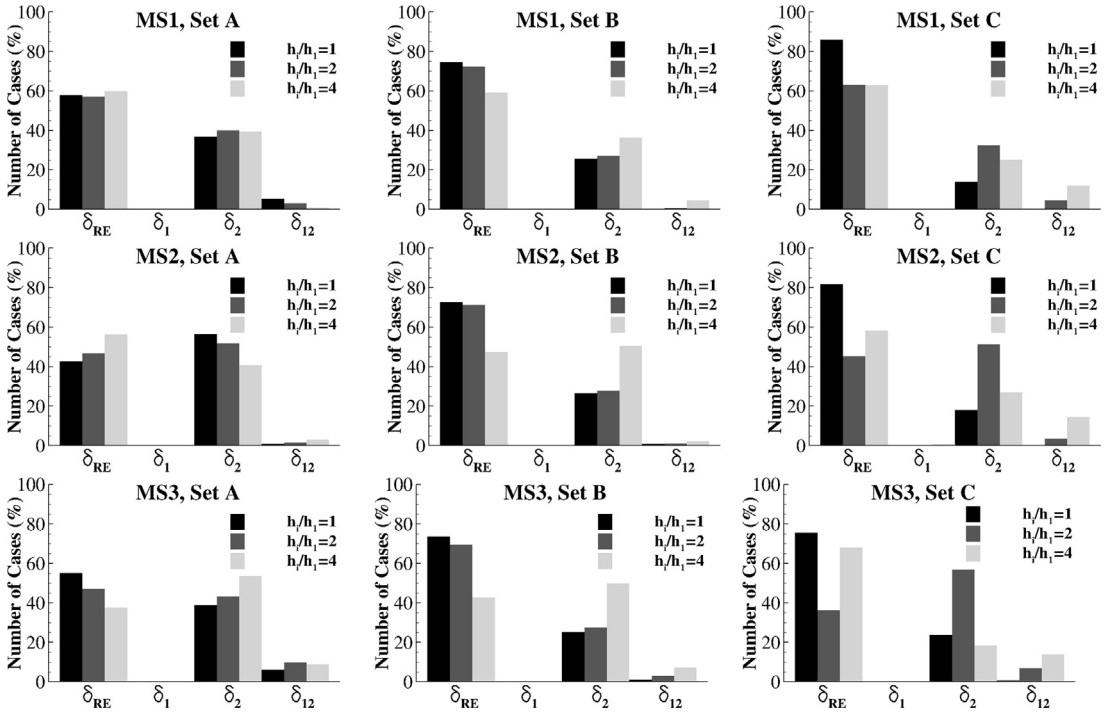

Fig. 6. Distribution of the number of cases that a specific error estimator is invoked. Horizontal velocity component u_x of the manufactured solutions.

uncertainty of the mean flow quantities, horizontal u_x and vertical u_y velocity components and pressure coefficient C_p. In this case, we have calculated the ratio between the estimated uncertainties for $h_i/h_1 = 1$, $h_i/h_1 = 2$ and $h_i/h_1 = 4$ and the exact error ratio $F_e = U_\phi/e_\phi$ for the three grid sets and the three MS's. As expected (due to the absence of scatter), none of the estimated uncertainties presented $F_\sigma > 1$.

None of the estimated uncertainties is below the exact error. Although there are some small differences between the results for the three mean flow quantities, we will illustrate the results for the horizontal velocity component u_x only. Fig. 6 presents the distribution of the number of cases that a particular error estimator is used. Although the trends are not exactly equal for the three grids sets and the three MS's, there are some overall tendencies in the data:

- Most of the errors are estimated with the observed p (δ_{RE}) and with $p = 2$ (δ_2). Although not systematically, the number of cases based on δ_{RE} tends to decrease with the grid coarsening, whereas the opposite trend is observed for δ_2.
- The number of error estimations based on a power series with two terms and fixed exponents (δ_{12}) is rather small. However, this number tends to increase with the grid coarsening.
- None of the error estimations was based on the single term expansion with $p = 1$ (δ_1).

Fig. 7 presents the histograms of F_e for the horizontal velocity component u_x. For the finest grids ($1 \leqslant h_i/h_1 \leqslant 2$), the majority of cases exhibits $1 \leqslant F_e < 2$, irrespective of the grid set and the kind of manufactured solution. It is clear that F_e tends to increase with the grid coarsening, but the number of cases with $F_e \geqslant 8$ tends to be small. The exception is grid set C where the values of F_e obtained for the coarsest grids ($4 \leqslant h_i/h_1 \leqslant 8$) are clearly larger than those obtained for the other two grid sets. This is again an indication that the level of accuracy of a numerical calculation is not solely determined by the total number of grid nodes, but also by the grid type.

4.2. Flow over a flat plate

The second test case is the two-dimensional, incompressible, statistically-steady flow over a flat plate. The computational domain is rectangular with the inlet, outlet and external boundaries sufficiently away from the plate (see Appendix C) to guarantee that the results are not affected by the limited domain size [21,22].

Calculations were performed for Reynolds numbers of $Re = 10^7$, $Re = 10^8$ and $Re = 10^9$, with $Re_L = \frac{U_\infty L}{\nu}$, where U_∞ is the undisturbed velocity, L is the length of the plate and ν is the kinematic viscosity of the fluid. As for the previous test case, all results presented below use dimensionless variables obtained with L and U_∞ as the reference length and velocity. We have made calculations with two eddy-viscosity models: the Spalart and Allmaras (SPAL) one-equation model [23] and the Shear-Stress Transport (SST) $k-\omega$ two-equation model [24].

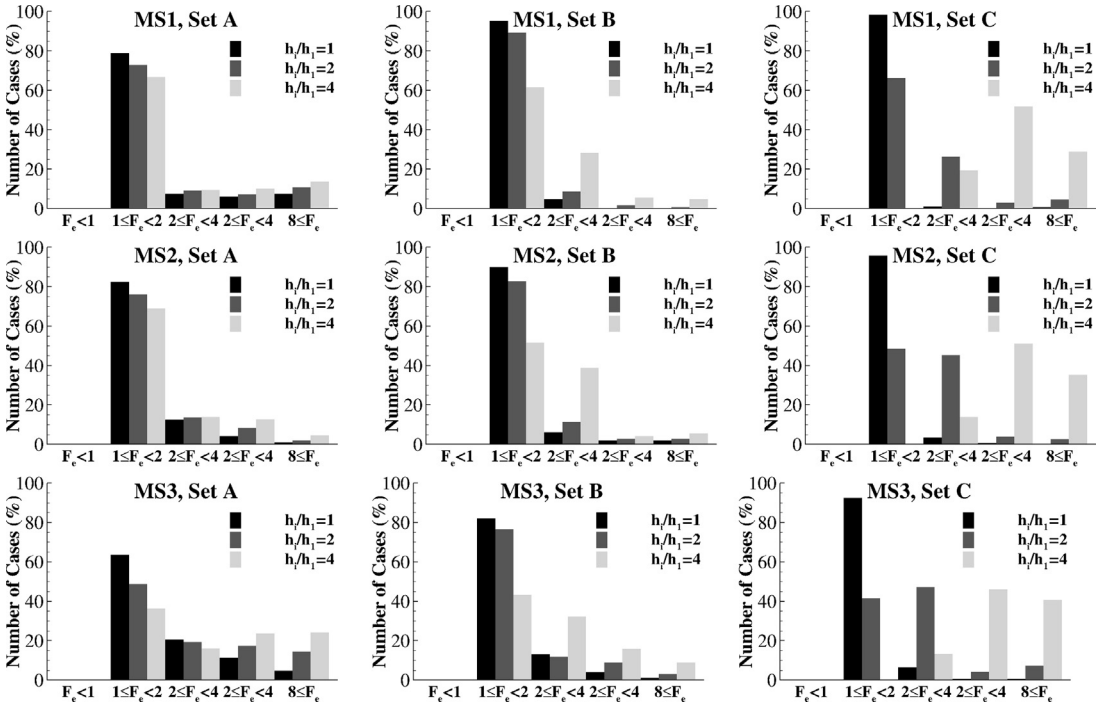

Fig. 7. Ratio between the estimated uncertainties and the exact error $F_e = U_{u_x}/e_{u_x}$ of the horizontal velocity component u_x. Manufactured solutions.

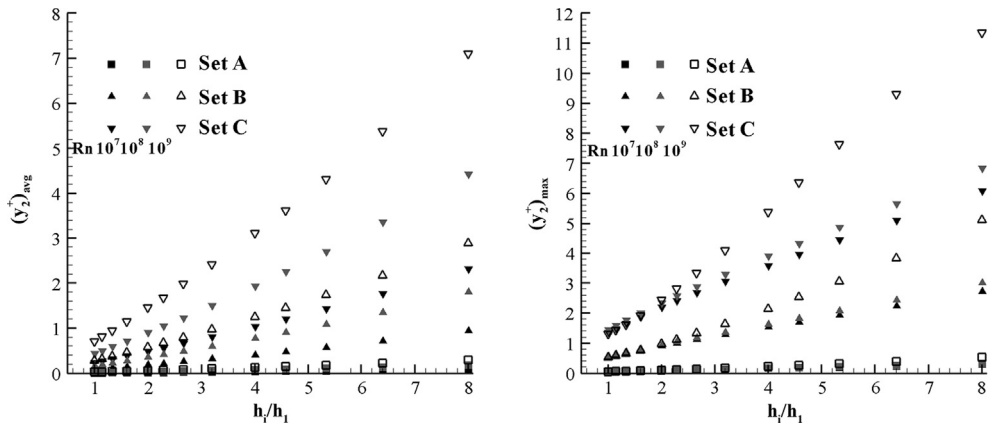

Fig. 8. Maximum and average dimensionless distance in wall coordinates at the first grid node away from the wall y_2^+ as a function of the grid refinement ratio.

For each Reynolds number, we have generated three sets of 13 geometrically similar Cartesian grids (the definition of h_i/h_1 given by Eq. (22) is still valid). The three grids sets cover a grid refinement ratio of 8 and each set contains 3 grids between each doubling of the grid spacing, i.e. there are three groups of 5 grids, each covering a grid refinement ratio of 2. As for the previous test case, the three sets have different near-wall grid line distances. Fig. 8 presents the maximum and the average non-dimensional distance to the wall y_2^+ at the first grid node away from the plate for all the calculations performed. The results correspond to the SPAL model, but similar results are obtained for the SST model. All the grids of set A have $(y_2^+)_{\max} < 1$, whereas all the grids of set C have $(y_2^+)_{\max} > 1$.

As for the previous case, calculations were performed with the finite-difference 2D-flow version of PARNASSOS [20] with 15 digits precision and the iterative error was reduced to machine accuracy.

We have checked the consistency of the uncertainty estimations for $h_i/h_1 = 1$, $h_i/h_1 = 2$ and $h_i/h_1 = 4$ in the three grids sets (A, B and C) for each turbulence model (SPAL and SST) and Reynolds number (10^7, 10^8 and 10^9).

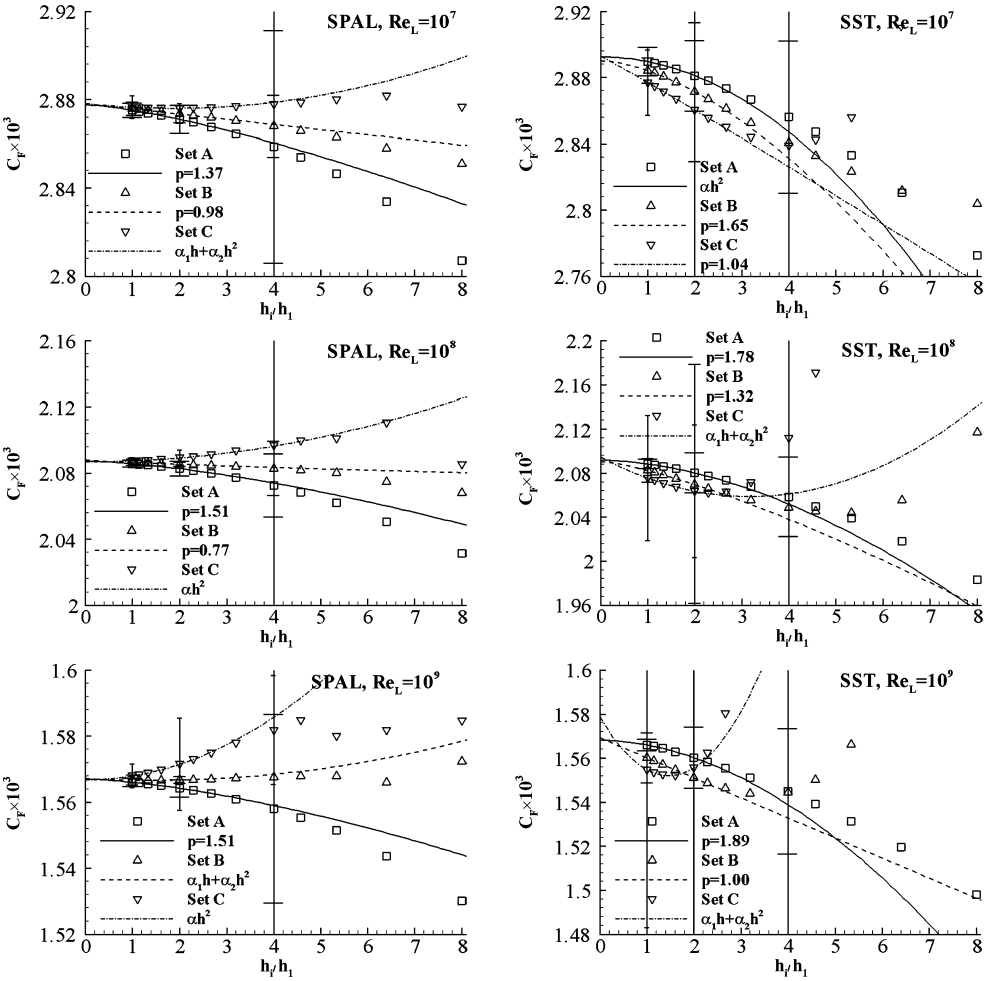

Fig. 9. Convergence of the friction resistance coefficient C_F with the grid refinement ratio. Fits obtained from the data with $1 \leqslant h_i/h_1 \leqslant 2$. Turbulent flow over a flat plate.

We have selected the same four integral quantities as in the previous test case: C_F, δ^*, θ and H. Naturally, C_F is determined with[6] $0 \leqslant x \leqslant 1$ and in this case δ^*, θ and H are determined at $x = 0.5$.

The convergence of C_F with the grid refinement is depicted in Fig. 9. The convergence properties are dependent on the turbulence model, grid set and Reynolds number. Not all the cases exhibit monotonic convergence and it is clear that most of the data with $h_i/h_1 > 4$ are outside the "asymptotic range". Nevertheless, all the estimated error bars are consistent, i.e. for a given turbulence model and Reynolds number, the 9 error bars estimated for the three grid refinement ratios and three grid sets have a region of overlap.

Figs. 10 to 12 present the convergence of δ^*, θ and H at $x = 0.5$ with the grid refinement ratio. The results confirm the trends observed for C_F, i.e. the convergence properties depend on the selected turbulence model, grid set and Reynolds number. Furthermore, the data show that the convergence properties depend on the selected flow variable. For all flow variables, turbulence model and Reynolds number, there is overlap between the estimated error bars for the three grid sets and three levels of grid refinement, which confirms the consistency of the results obtained with the proposed procedure.

We observe that none of the fits for C_F, δ^*, θ and H exhibited $F_\sigma > 1$, which is perhaps not a very surprising result for this simple geometry. However, most of the error estimates performed for the data included in Figs. 9 to 12 were not based on δ_{RE}, including several of those made for $h_i/h_1 = 1$. Therefore, the alternative error estimators play a significant role in the uncertainty estimation of functional quantities of a "simple practical flow", i.e. a flow over a flat plate at high Reynolds numbers.

For each Re_L and turbulence model and grid set, we have also checked the consistency of the mean flow quantities, u_x, u_y and C_p and eddy-viscosity ν_t error bars obtained for three grid densities at 1045 (95×11) locations. We have even

[6] We recall that x is a dimensionless quantity $x = X/L$.

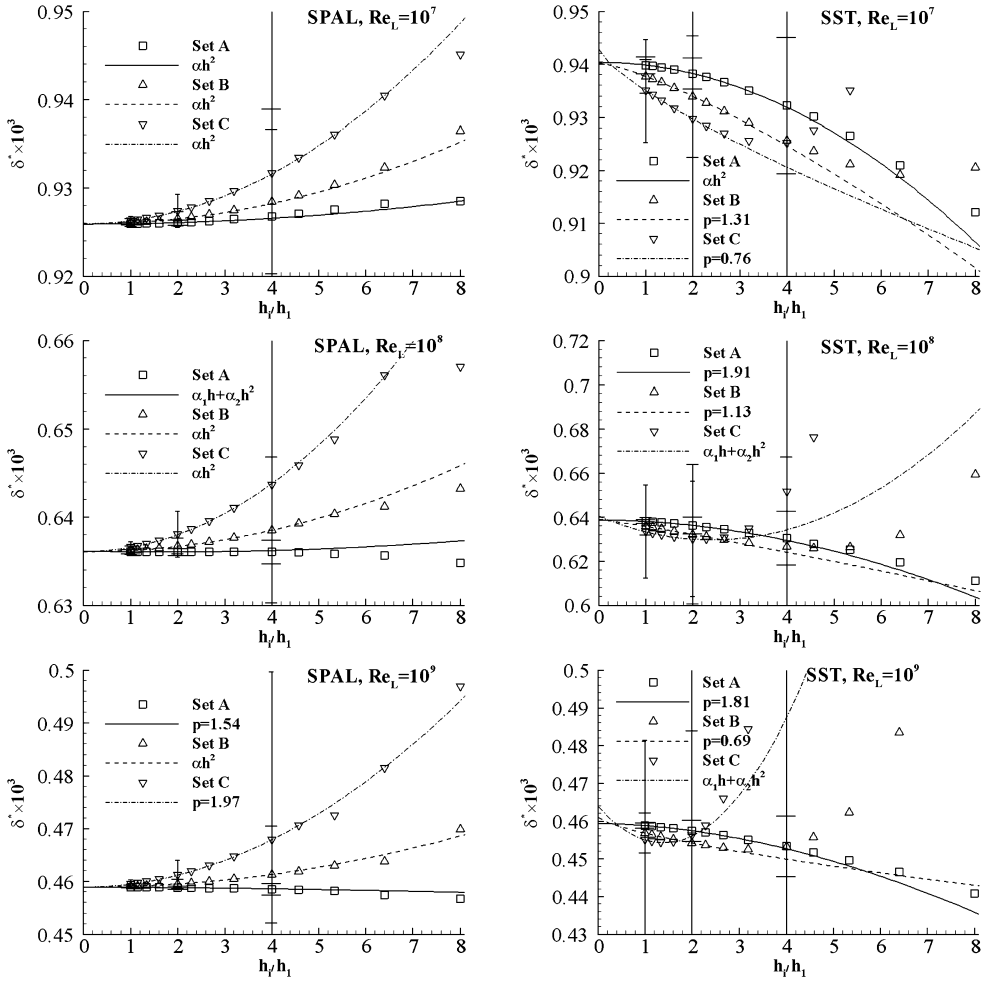

Fig. 10. Convergence of the displacement thickness δ^* at $x = 0.5$ with the grid refinement ratio. Fits obtained from the data with $1 \leqslant h_i/h_1 \leqslant 2$. Turbulent flow over a flat plate.

checked the consistency between error bars obtained for different grid sets where local quantities were determined with second-order polynomial interpolations[7] at fixed locations not coinciding with grid nodes.

As for the previous test case, we have started by determining the number of cases that a given error estimator was used. Figs. 13–16 illustrate these distributions for the horizontal velocity component u_x and for the eddy-viscosity ν_t. Although the results are not exactly equal for all the conditions tested, there are some clear trends:

- The results obtained for u_x and ν_t with both turbulence models are similar for most of the cases tested. The main exception is grid set C for $Re_L = 10^8$ and $Re_L = 10^9$, where the SST model exhibits a very small number of uncertainty estimations based on δ_{RE} for u_x. This is likely a consequence of the too large values of y_2^+ of most of the grids of this set.
- Most of the uncertainty estimations for $h_i/h_1 = 1$ are based on δ_{RE} (followed by δ_2). With grid coarsening, this number decreases, especially for $h_i/h_1 = 4$.
- The number of cases based on δ_{12} increases with the grid coarsening.
- The expansion with one linear term δ_1 is the least selected.
- There are some cases with $F_\sigma > 1$, which are mainly obtained for $h_i/h_1 = 4$. Therefore, it is likely that some of them are a consequence of the use of data from too coarse grids and not really of scatter in the data. In contrast, the u_x results obtained in grid sets A with the SST model show the largest number of cases with $F_\sigma > 1$ for $h_i/h_1 = 1$, which suggests the existence of some scatter in the data.

[7] 2-D cubic polynomial was also tested and the results obtained are equivalent to those presented in the paper.

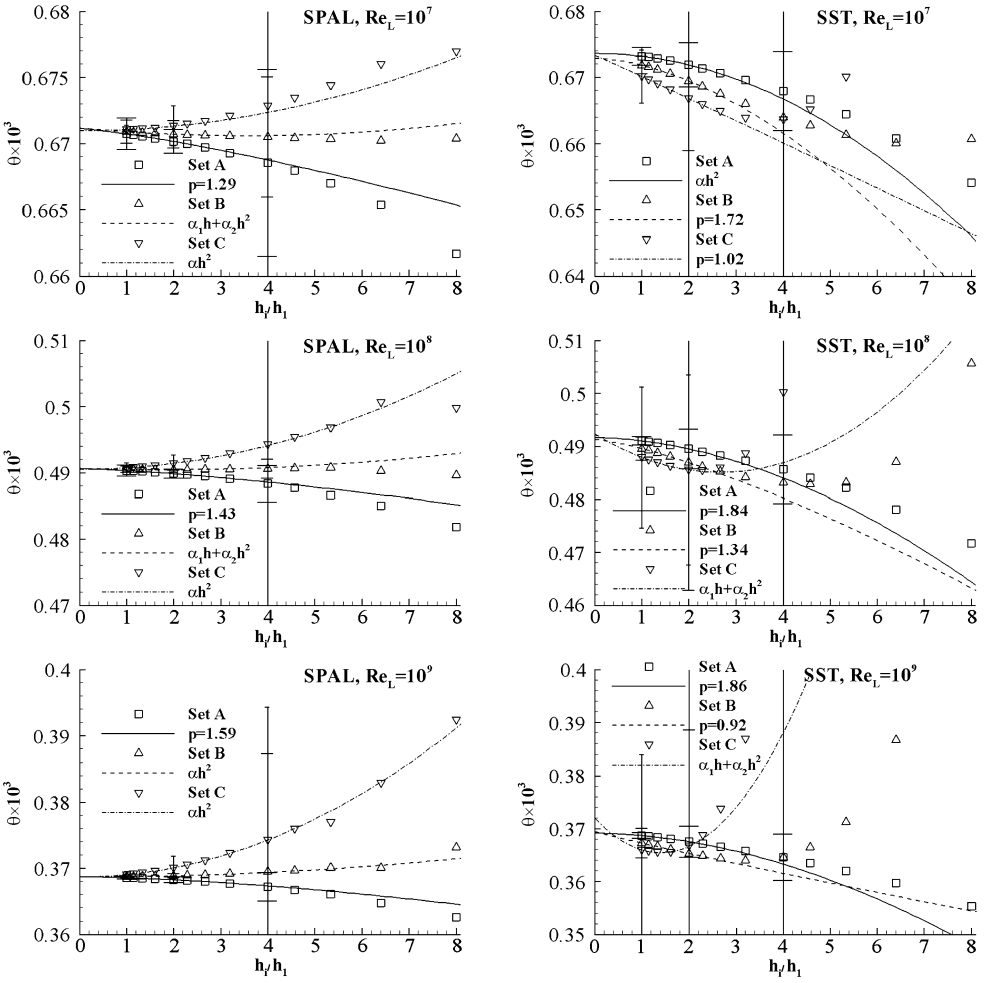

Fig. 11. Convergence of the momentum thickness θ at $x = 0.5$ with the grid refinement ratio. Fits obtained from the data with $1 \leqslant h_i/h_1 \leqslant 2$. Turbulent flow over a flat plate.

These trends confirm the importance of the error estimations based on power series expansions with fixed exponents for practical applications, especially for the coarsest grids.

The number of cases with non-overlapping error bars at the 1045 locations selected is given in Fig. 17 for the mean flow quantities u_x, u_y and C_p and for the eddy-viscosity ν_t. We have performed twelve checks for each turbulence model and Reynolds number. For each grid set (A, B and C) and for all grid sets (G) we have made three different comparisons: the error bars at $h_i/h_1 = 1$ and $h_i/h_1 = 2$ ($_{12}$); the error bars at $h_i/h_1 = 1$, $h_i/h_1 = 2$ and $h_i/h_1 = 4$ ($_{13}$) and the same as the previous but with the safety factor equal to 3 for the coarsest grids ($_{13c}$).

For most of the cases, the number of instances with non-overlapping error bars is significantly smaller than the target value of 5%. There are only seven comparisons that exhibit a number of inconsistent error bars larger than the 5% target and they all correspond to comparisons between error bars of the three grid sets (G) at $Re_L = 10^7$ (top plots of Fig. 17). Nevertheless, it is clear that the number of inconsistent error bars decreases when the grids with $h_i/h_1 > 4$ are assumed to be outside the "asymptotic range" (comparison between G_{13} and G_{13c} that assumes $F_s = 3$). We must bear in mind that the coarsest grids of sets C (in particular at $Re_L = 10^9$) present unreasonably large values of y_2^+ (see Fig. 8) and so the performance of the proposed procedure is actually surprisingly good.

4.3. Flow over a backward facing step

The flow over a backward facing step has been one of the test cases of the three Lisbon Workshops on Verification [9–11]. The Reynolds number based on the step height and the velocity of the incoming flow, U_{ref}, is 5×10^5 and the present calculations have been reported in [17]. In this paper, we will restrict ourselves to the results obtained with the Spalart–Allmaras one-equation model [23] and with the SST $k-\omega$ two-equation model [24].

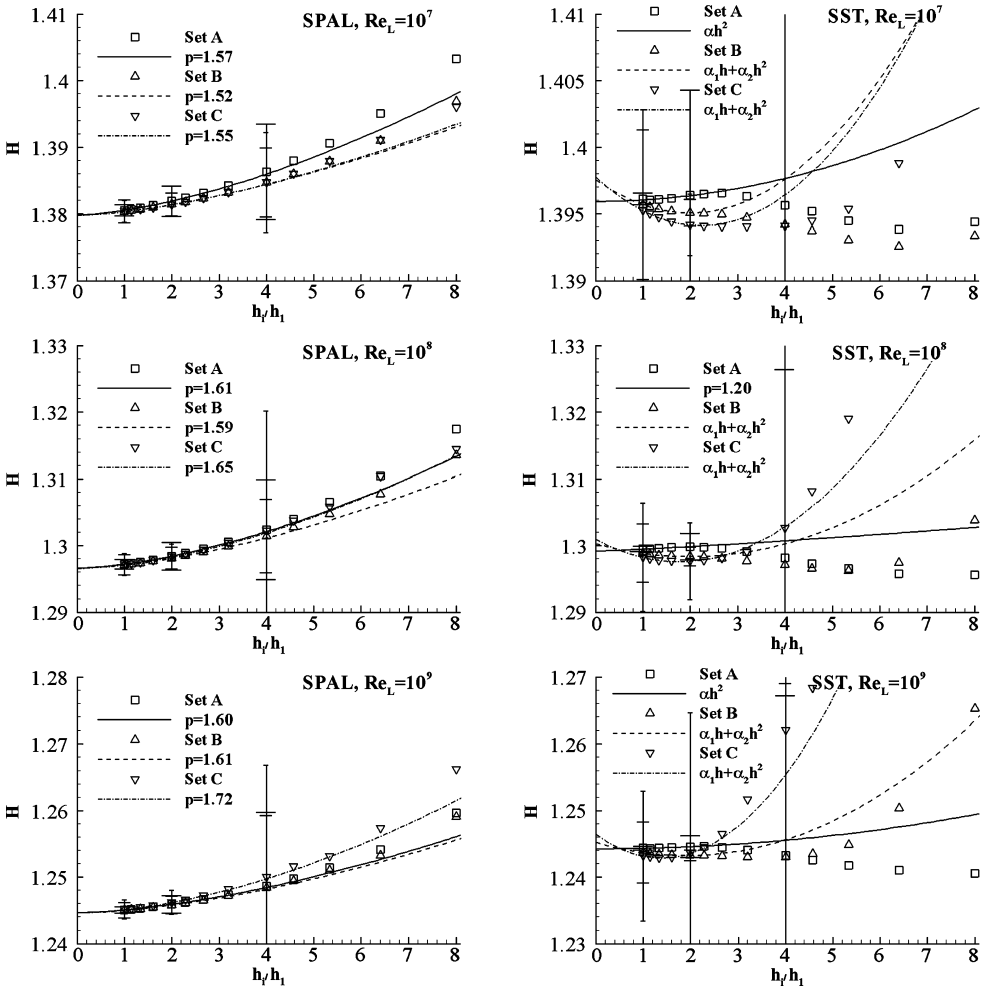

Fig. 12. Convergence of the shape factor H at $x = 0.5$ with the grid refinement ratio. Fits obtained from the data with $1 \leqslant h_i/h_1 \leqslant 2$. Turbulent flow over a flat plate.

There are two sets of 19 single-block, structured, geometrically similar grids, A and B, with coarsest grids of 41×41 nodes and finest grids of 401×401 nodes covering a grid refinement ratio of 10. Therefore, the definition of h_i/h_1 of the two previous test cases (Eq. (22)) also applies to this example. The grids in the vicinity of the step are illustrated in Fig. 18.

As for the previous examples, all the calculations were carried out with the finite-difference, 2D-flow version of PARNASSOS [20] using 15-digits precision and reducing the iterative error to machine accuracy.

We have estimated the uncertainty of all selected flow quantities for three levels of grid refinement: $h_i/h_1 = 1$ using the data of the 11 finest grids covering a grid refinement ratio of 2; $h_i/h_1 = 2$ using the data of 6 grids covering a grid refinement ratio of 2 and $h_i/h_1 = 4$ based on the data of the 4 coarsest grids that cover a grid refinement ratio of 2.5.

The convergence of the friction resistance coefficient at the top ($(C_F)_T$) and bottom ($(C_F)_B$) walls and the pressure resistance coefficient (base drag) at the bottom wall ($(C_P)_B$) with the grid refinement is depicted in Fig. 19.

As for the previous test cases, the convergence properties depend on the selected flow quantity, turbulence model and grid set and the convergence is not always monotonic. The estimated error bars are once more consistent, showing overlap between the three levels of grid refinement and the two grid sets for all cases. In this case, the use of an error estimation based on δ_{RE} is the exception, which illustrates the need for alternative error estimators in practical calculations.

As for the flat plate flow, we have estimated the uncertainty of the mean flow quantities u_x, u_y and C_p and of the eddy-viscosity ν_t at 361 nodes common to all grids of set A (in the grids with $h_i/h_1 \leqslant 4$). Second-order interpolation is used for the data of set B to obtain the uncertainties in the same locations.

Fig. 20 presents the distribution of the number of cases based on each of the four error estimators for the horizontal u_x and vertical u_y velocity components and for the eddy-viscosity ν_t. The distributions obtained for the two grid sets are similar and the most striking feature is the large number of cases using δ_{12} and the relatively small number of cases using δ_{RE}. Furthermore, the largest number of cases with $F_\sigma > 1$ is systematically obtained for $h_i/h_1 = 1$. This suggests the

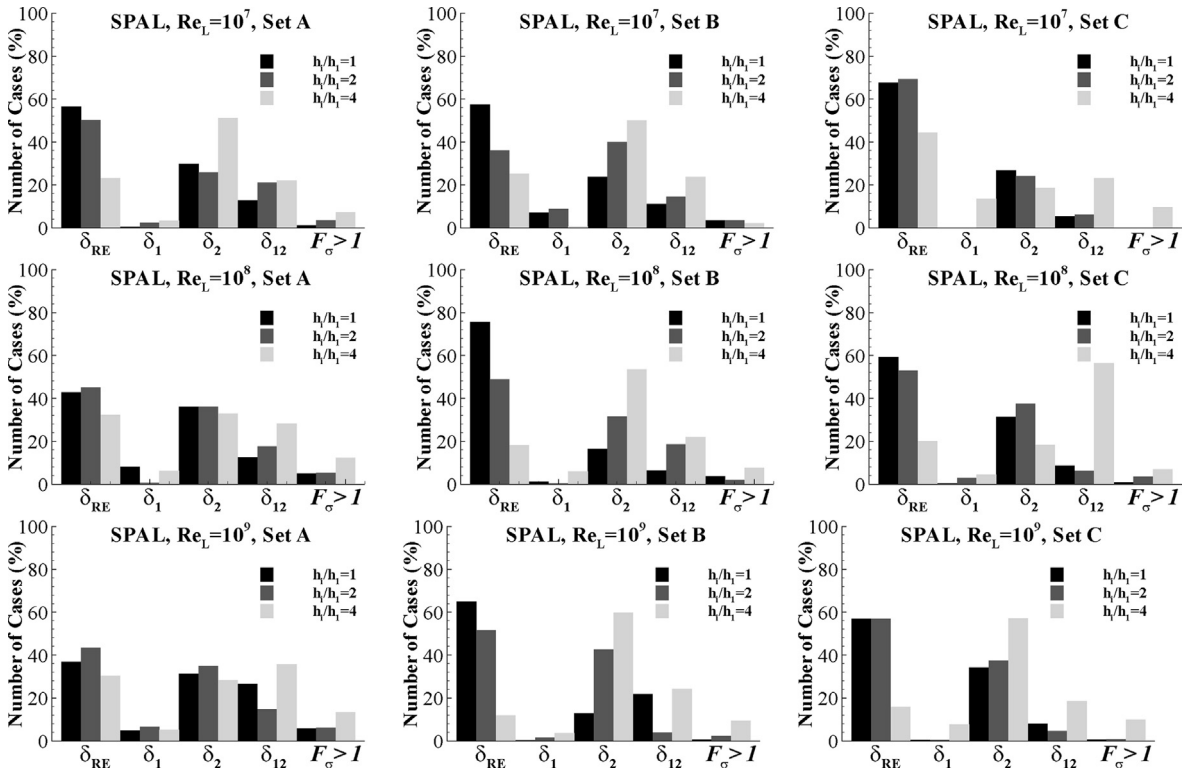

Fig. 13. Distribution of the number of cases based on each error estimator. Horizontal velocity component u_x. Spalart–Allmaras one-equation model. Turbulent flow over a flat plate.

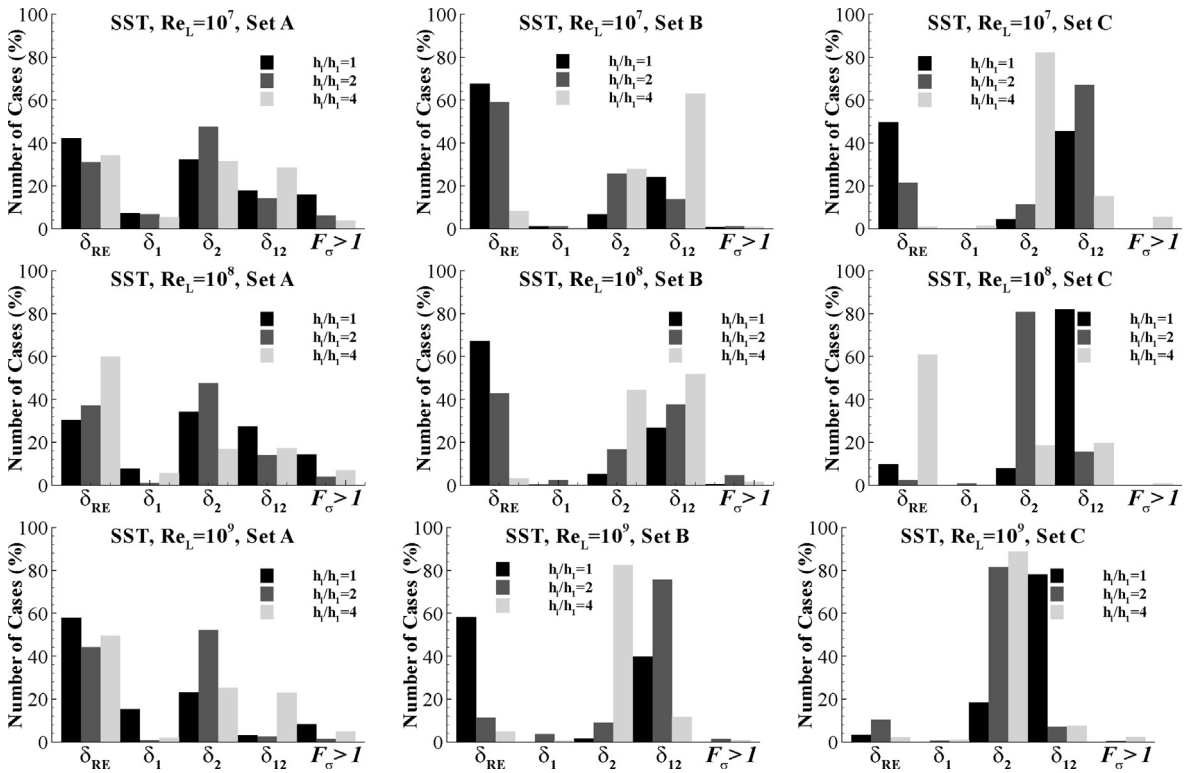

Fig. 14. Distribution of the number of cases based on each error estimator. Horizontal velocity component u_x. SST $k-\omega$ two-equation model. Turbulent flow over a flat plate.

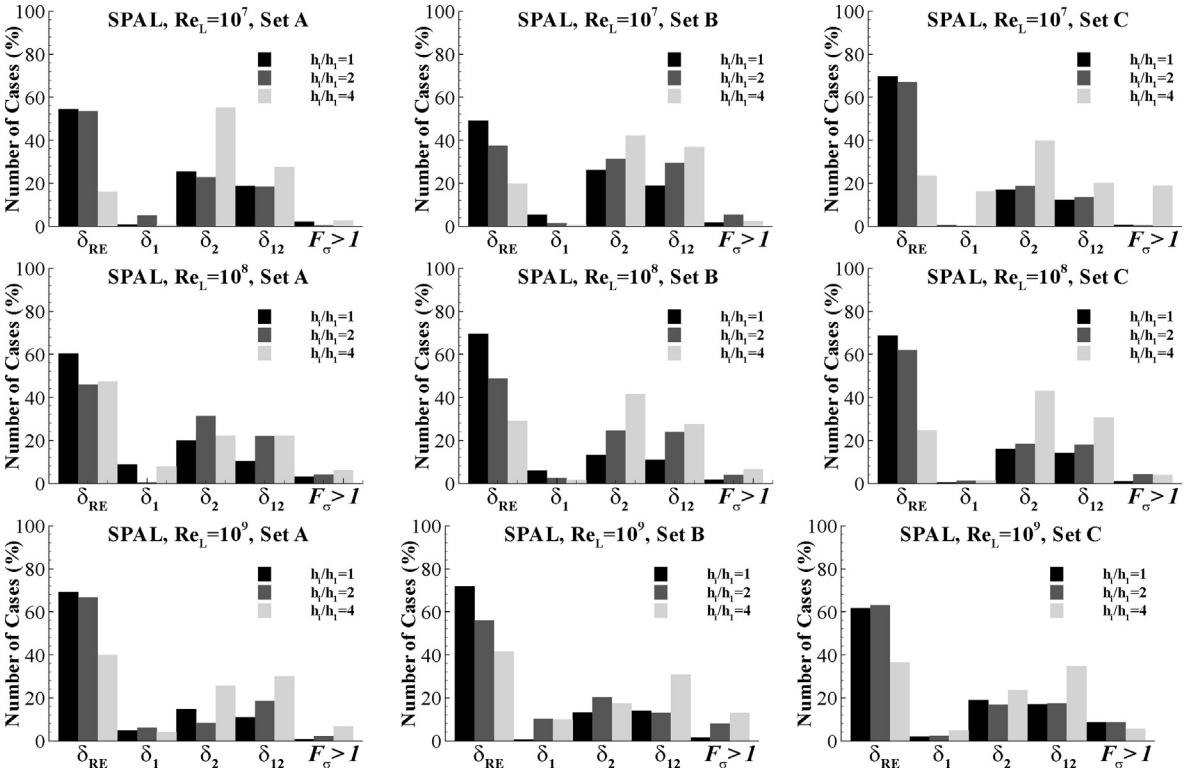

Fig. 15. Distribution of the number of cases based on each error estimator. Eddy-viscosity ν_t. Spalart–Allmaras one-equation model. Turbulent flow over a flat plate.

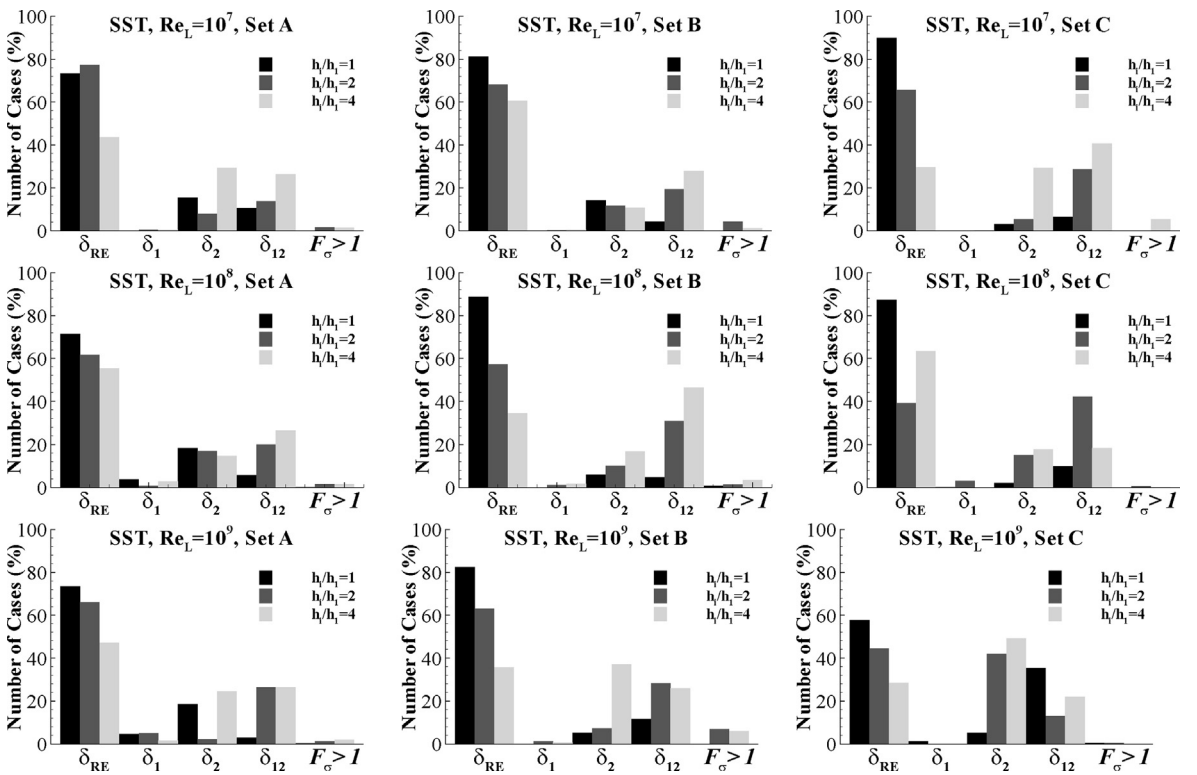

Fig. 16. Distribution of the number of cases based on each error estimator. Eddy-viscosity ν_t. SST $k-\omega$ two-equation model. Turbulent flow over a flat plate.

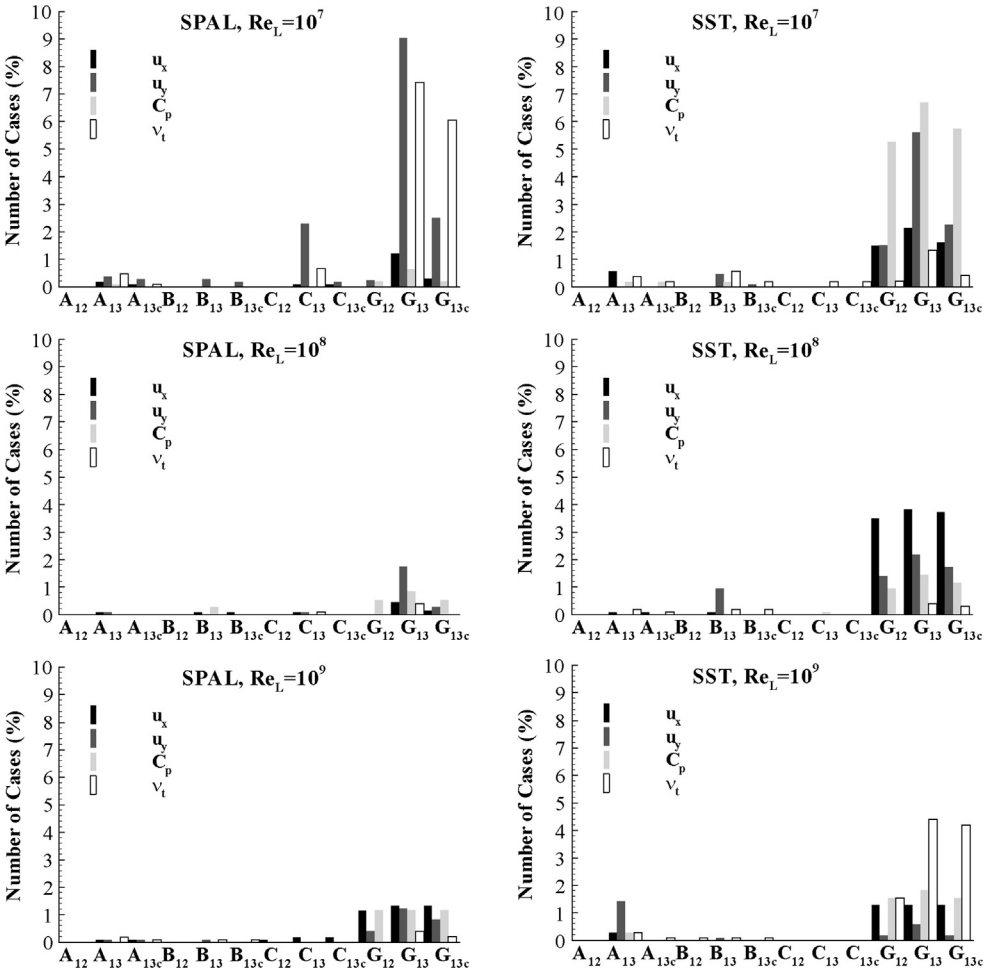

Fig. 17. Distribution of the number of cases with non-overlapping error bars of mean flow quantities, u_x, u_y and C_p and eddy-viscosity ν_t. G stands for all grid sets, $_{12}$ for error bars of $h_i/h_1 = 1$ and $h_i/h_1 = 2$, $_{13}$ for error bars of $h_i/h_1 = 1$, $h_i/h_1 = 2$ and $h_i/h_1 = 4$, $_{13c}$ same as $_{13}$ but with the safety factor equal to 3 for the coarsest grids. Turbulent flow over a flat plate.

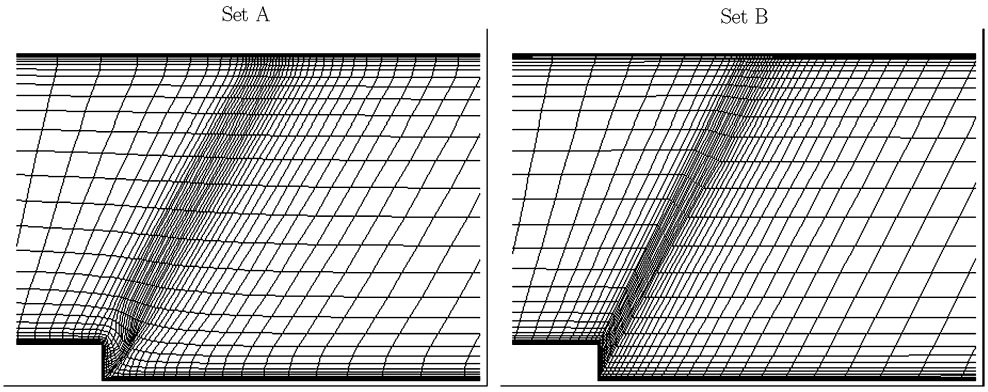

Fig. 18. Illustration of the two grids sets for the calculation of the flow over a backward facing step.

existence of a significant amount of scatter in the data. Most likely, this is due to the (deliberate [9–11]) lack of quality of the grids of both sets.

The number of cases with non-overlapping error bars at the 361 locations selected is given in Fig. 21 for the mean flow quantities u_x, u_y and C_p and for the eddy-viscosity ν_t. The nomenclature is identical to that defined above for the flat plate flow, but in this case we only have nine checks for each turbulence model, because there are only two grid sets.

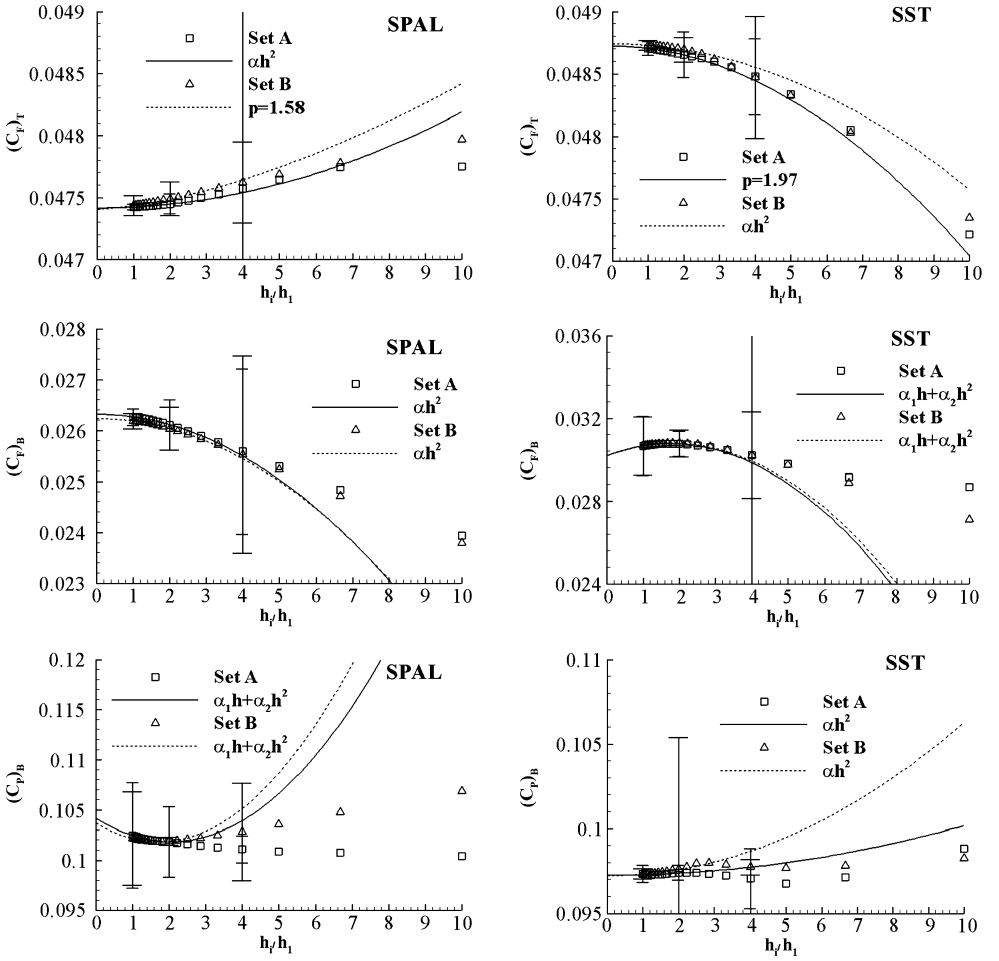

Fig. 19. Convergence of the friction resistance coefficient at the top $(C_F)_T$ and bottom $(C_F)_B$ walls and pressure resistance coefficient (base drag) at the bottom wall $(C_P)_B$ with the grid refinement ratio. Fits obtained from the data with $1 \leqslant h_i/h_1 \leqslant 2$. Turbulent flow over a backward facing step.

The results are clearly dependent on the turbulence model. For the SST model, all checks produce a number of "failures" below 5%. Assuming the data of the four coarsest grids to be outside the "asymptotic range" leads to a clear reduction of the number of inconsistent error bars. The same trend is observed in the SPAL data. However, in this case only the comparisons between the mean flow variables error bars of $h_i/h_1 = 1$ and $h_i/h_1 = 2$ lead to a number of "failures" below 5% for all cases. The comparisons between error bars of the three refinement levels and two grid sets fail to meet the 5% target for all variables except the pressure coefficient. However, it must be recognized that the coarsest grids of the two sets are really too coarse to capture any flow details, which leads to meaningless changes between the flow fields obtained for coarsest grids levels. In these conditions, it is impossible to expect a reasonable performance from a method based on grid refinement studies.

4.4. Flow around a tanker

The final example is the flow around the KVLCC2 tanker at model scale Reynolds number (4.6×10^6). It is a practical test case, which has been employed for the last three Workshops on Numerical Ship Hydrodynamics [27–29].

We have selected a computational domain with a cylindrical shape where we have generated four sets (A, B, C and D) of six nearly geometrically similar grids (using exactly the same settings in the grid generators for each family of grids). All the grids are single-block H–O grids that differ essentially in the streamwise and girthwise node distributions. Although the grids do not respect exact geometric similarity (especially at the bow and stern contours), h_i/h_1 is again defined by Eq. (22). The coarsest grids have 0.7 to 0.8 million cells and the finest 5.3 to 6.1 million cells, covering always a grid refinement ratio of 2. It is noted that the grids near-wall distance ensures a maximum y_2^+ below 0.8 in all 24 grids. Fig. 22 illustrates the grids on the ship surface using only half the nodes of the coarsest grids of each set.

The calculations were made with the three-dimensional version of PARNASSOS [30,31] using the SST $k-\omega$ two-equation eddy-viscosity turbulence model [24]. We have used 15 digits precision, but we have not converged all solutions to machine

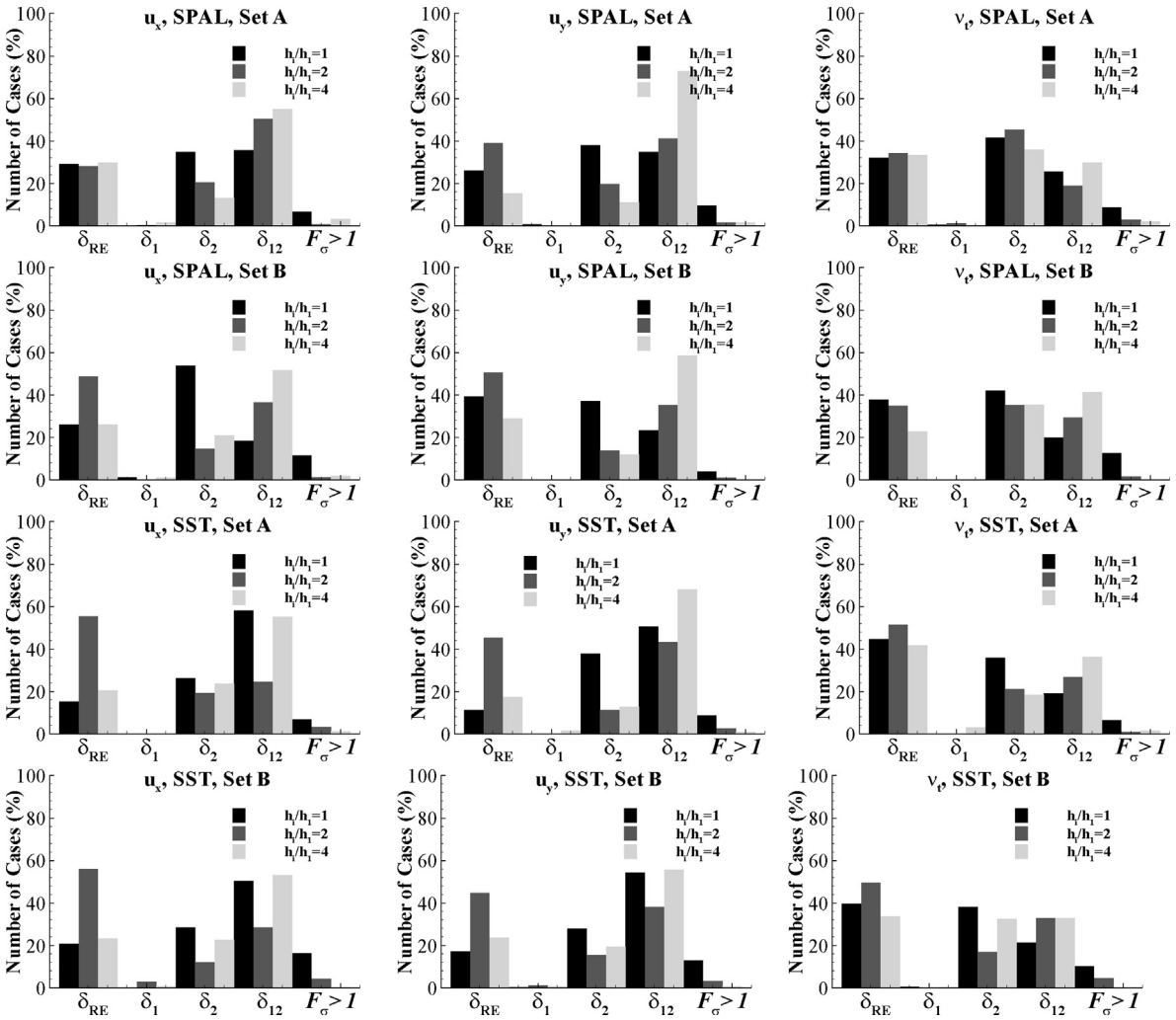

Fig. 20. Distribution of the number of cases based on each error estimator. Horizontal u_x and vertical u_y velocity components and eddy-viscosity ν_t. Turbulent flow over a backward facing step.

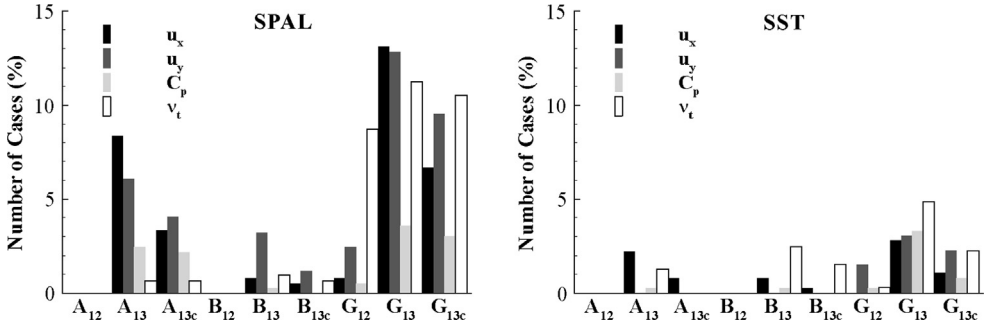

Fig. 21. Distribution of the number cases with non-overlapping error bars of mean flow quantities, u_x, u_y and C_p and eddy-viscosity ν_t. G stands for all grid sets, $_{12}$ for error bars of $h_i/h_1 = 1$ and $h_i/h_1 = 2$, $_{13}$ for error bars of $h_i/h_1 = 1$, $h_i/h_1 = 2$ and $h_i/h_1 = 4$, $_{13c}$ same as $_{13}$ but with the safety factor equal to 3 for the coarsest grids. Turbulent flow over a backward facing step.

accuracy. We have ensured, though, that the iterative error was reduced to at least three orders of magnitude below the discretization error [12].

We have chosen four integral flow quantities to check the consistency of the proposed procedure: the friction resistance coefficient C_F; the pressure resistance coefficient C_P; the viscous resistance coefficient C_V and the nominal wake fraction coefficient W_f. C_F and C_P require the integration of the shear-stress and pressure coefficient on the ship surface, which has

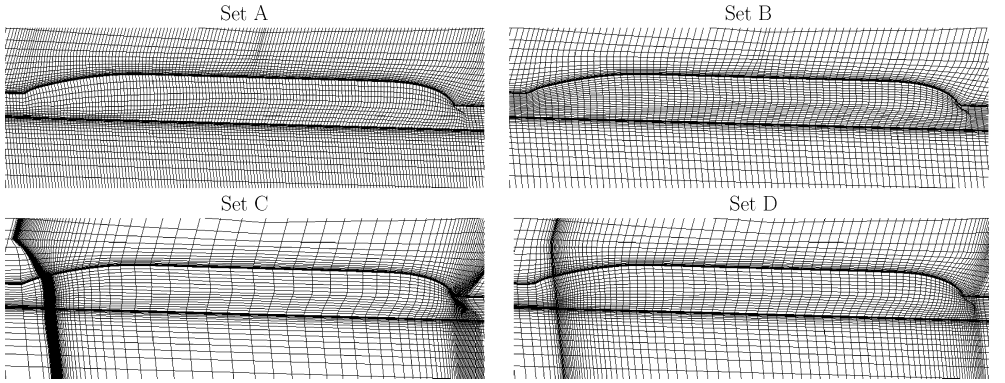

Fig. 22. Illustration of the four grids sets for the calculation of the flow around the KVLCC2 tanker at model scale Reynolds number.

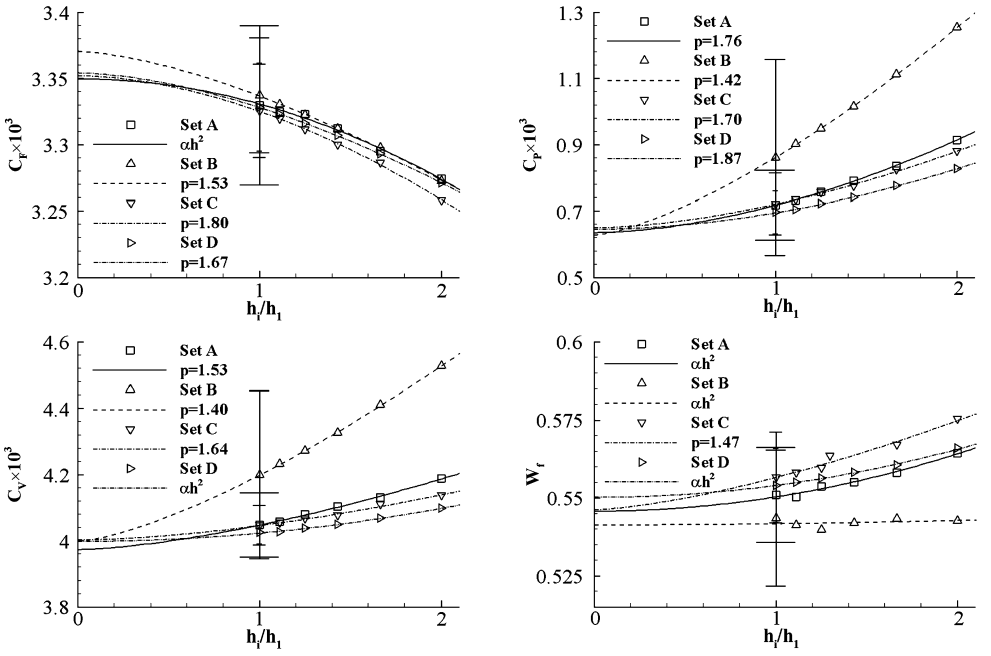

Fig. 23. Convergence of the friction C_F and pressure C_P and viscous C_V resistance coefficients and of the nominal wake fraction W_f with the grid refinement ratio. Fits obtained from the data with $1 \leqslant h_i/h_1 \leqslant 2$. Flow around the KVLCC2 tanker at model scale Reynolds number.

been done with a second-order Gauss quadrature rule. C_V is just the sum of C_F and C_P and W_f requires the integration of the axial velocity u_x at the propeller disc (located at $x = 0.9825 L_{PP}$), for which the same numerical integration technique was applied as for C_F and C_P.

Fig. 23 presents convergence of C_F, C_P, C_V and W_f with the grid refinement. The results show a small sensitivity of C_F to the grid node distribution. On the other hand, C_P (and consequently C_V) is significantly affected by the selected grid set with the smallest uncertainty obtained for set D and the largest for set B (having the largest streamwise spacing at the bow and stern contours). Nevertheless, all resistance coefficients converge monotonically with observed orders of grid convergence within the expected range. Therefore, it is no surprise that the four error bars overlap for C_F, C_P and C_V.

The convergence of the nominal wake fraction coefficient W_f exhibits more scatter than the resistance coefficients, with the exception of set D. This is a consequence of the local streamwise grid line spacing and grid quality (skewness and orthogonality), which are significantly better in set D than in all the other sets (sets A and B do not have clustering of grid nodes at the propeller plane and set C contains highly distorted grids). The proposed procedure leads to four overlapping error bars, which is a remarkable result because the data of set B (with the largest streamwise spacing) show clearly an anomalous behaviour with only minor changes in W_f for the three finest grids.

The convergence of local flow quantities was checked at the propeller plane ($x = 0.09825 L_{PP}$) for 654 locations (which are the locations where measurements were made [27,29]). Understandably, these locations do not coincide with grid nodes; second-order polynomial interpolation was applied to obtain the local values of the mean velocity components u_x, u_y and u_z, the pressure coefficient C_p and the eddy-viscosity ν_t.

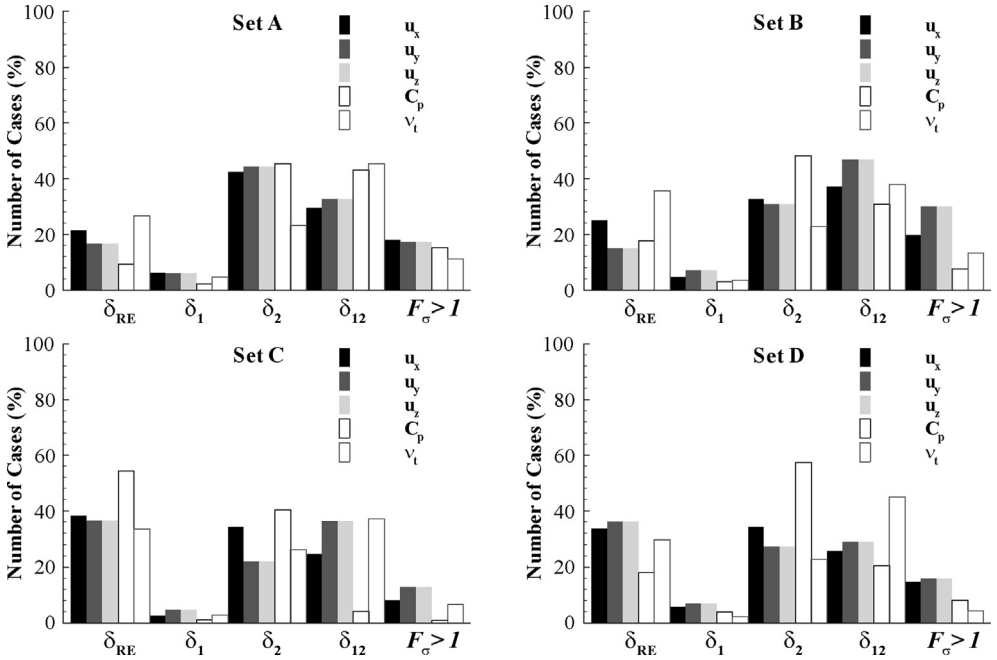

Fig. 24. Distribution of the number of cases that a specific error estimator is invoked. Axial u_x, horizontal u_y and vertical u_z velocity components, pressure coefficient C_p and eddy-viscosity ν_t at the propeller plane, $x = 0.9825 L_{PP}$. Flow around the KVLCC2 tanker at model scale Reynolds number.

The number of cases that each error estimator is called is given in Fig. 24. It is clear that δ_{RE} is least called for sets A and B that include the grids with the largest streamwise grid line spacing. This tendency is accompanied with a significant number of locations where the error is estimated with δ_{12}, which is a trend also valid for the other two grid sets. Furthermore, there is also a significant number of cases that exhibit $F_\sigma > 1$, which in some cases reaches values above 20%. These numbers reflect the difficulties to estimate errors based on power series expansions for the so-called "practical applications". Nevertheless, with the proposed procedure to estimate numerical uncertainty, the number of locations with overlapping error bars for the four grid sets is always above 95%. The number of "failures" is 1.68% for u_x, 1.07% for u_y, 0.46% for u_z, 1.84% for C_p and 2.91% for ν_t.

5. Final remarks

A procedure has been presented for the estimation of the numerical uncertainty of any integral or local flow quantity, based on grid refinement studies. The uncertainty is determined by an error estimation multiplied by a safety factor.

The error is estimated with power series expansions as a function of the typical cell size, which are fitted to the data in the least-squares sense. Several alternative formulations are involved, including weighted and non-weighted fits of expressions with different exponents in the leading term of the series. The selection of the best error estimate is based on the standard deviation of the fits.

The choice of the safety factor follows the Grid Convergence Index, i.e. factor of safety equal to 1.25 for reliable error estimations and 3 for all other conditions. A reliable error estimation requires monotonic convergence with an observed order of grid convergence within a given range and a standard deviation of the fit smaller than an averaged data range parameter. For well controlled situations, i.e. monotonic convergence with the expected observed order of grid convergence and no scatter in the data, the method reduces to the well known Grid Convergence Index.

Four examples of application are presented ranging from the well controlled environment of manufactured solutions to the "practical calculation" of the flow around a tanker. An excellent performance of the proposed procedure is obtained for the manufactured solutions. Although the three solutions tested involve a fairly complex flow, the computational domain is simply a rectangle. This allows the use of strictly geometrically similar orthogonal grids, which makes it a less demanding test case.

For the other test cases there are no analytical solutions available, but we checked the proposed procedure for consistency, i.e. the overlap of error bars obtained for different grid densities and/or grid families. In general, we have obtained results that satisfy the desired target of 95% of cases with consistent (or conservative in the case of the manufactured solutions) error bars, but not for all the cases tested. The failures occur for error bars estimated for too coarse grids that in some cases are hardly able to capture the main flow features. Of course, one cannot expect a procedure based on grid refinement studies to produce a reliable error estimate when the solution is almost not changing due to the lack of grid resolution.

The results also show an increased number of cases that rely on the alternative power series expansions when the flow becomes more complex (geometry and flow details). It is further clear that scatter will be very hard to avoid in complex flows; the least-squares fits proposed in the present procedure are an effective way to deal with this problem. When the scatter level is comparable to the changes in the data, the present procedure may become too conservative. But such circumstances are supposed to be the exception and not the rule in uncertainty estimation based on grid refinement studies.

Appendix A. Summary of procedure for numerical uncertainty estimation

The present solution verification procedure estimates the uncertainty U_ϕ of a functional or local quantity ϕ from the data obtained in n_g grids, where n_g is supposed to be at least 4. The method is based on power series expansions that neglect high-order terms and assume that ϕ has at least second-order finite derivatives. It is also assumed that the lowest-order schemes used in the discretization are second or first-order accurate.

U_ϕ is determined from an error estimate ϵ_ϕ times a safety factor F_s. The steps to obtain $U(\phi)$ are summarized below.

1. Determination of ϵ_ϕ:
   - Solve
   $$\delta_{RE} = \alpha h_i^p$$
   in the least-squares sense with and without weights (see Appendix B) to obtain δ_{RE}, p and the standard deviations of the two fits σ. If any of fits exhibits $0.5 \leqslant p \leqslant 2$, $\epsilon_\phi = \delta_{RE}$. If both fits exhibit $0.5 \leqslant p \leqslant 2$, the value of δ_{RE} selected corresponds to the fit with the smallest standard deviation.
   - If the observed order of grid convergence $p > 2$, solve
   $$\delta_1 = \alpha h_i$$
   and
   $$\delta_2 = \alpha h_i^2$$
   in the least-squares sense with and without weights (see Appendix B) and determine the standard deviations of the four fits σ. ϵ_ϕ is obtained from the fit that exhibits the smallest standard deviation.
   - If the observed order of grid convergence $p < 0.5$ or impossible to establish, solve
   $$\delta_1 = \alpha h_i,$$
   $$\delta_2 = \alpha h_i^2$$
   and
   $$\delta_{12} = \alpha_1 h_i + \alpha_2 h_i^2$$
   in the least-squares sense with and without weights (see Appendix B) and determine the standard deviations of the six fits σ. ϵ_ϕ is obtained from the fit that exhibits the smallest standard deviation.
2. Determine a data range parameter
   $$\Delta_\phi = \frac{(\phi_i)_{\max} - (\phi_i)_{\min}}{n_g - 1}$$
   to assess the quality of the fit used to obtain the error estimate ϵ_ϕ.
3. Determine the safety factor from p, σ and Δ_ϕ:
   - If $0.5 \leqslant p < 2.1$ and $\sigma < \Delta_\phi$, $F_s = 1.25$.
   - Otherwise, $F_s = 3$.
4. Obtain the uncertainty from ϵ_ϕ and the safety factor F_s using the values of σ and Δ_ϕ to distinguish between "good" and "bad" error estimations:
   - For $\sigma < \Delta_\phi$:
   $$U_\phi(\phi_i) = F_s \epsilon_\phi(\phi_i) + \sigma + |\phi_i - \phi_{fit}|.$$
   - For $\sigma \geqslant \Delta_\phi$:
   $$U_\phi(\phi_i) = 3\frac{\sigma}{\Delta_\phi}\left(\epsilon_\phi(\phi_i) + \sigma + |\phi_i - \phi_{fit}|\right).$$

Appendix B. Least-squares solutions of power series expansions

B.1. Weights

The equations presented below are valid for least-squares solutions with and without weights.

- Non-weighted approach

$$w_i = 1 \quad \text{and} \quad nw_i = 1.$$

- Weighted approach

$$w_i = \frac{\frac{1}{h_i}}{\sum_{i=1}^{n_g} \frac{1}{h_i}} \quad \text{and} \quad nw_i = n_g w_i,$$

guaranteeing that

$$\sum_{i=1}^{n_g} w_i = 1.$$

B.2. Single term expansion with unknown order of grid convergence

ϕ_o, α and p are determined from the minimum of the function

$$S_{RE}(\phi_o, \alpha, p) = \sqrt{\sum_{i=1}^{n_g} w_i \left(\phi_i - \left(\phi_o + \alpha h_i^p\right)\right)^2}$$

that is obtained from

$$\frac{\partial S_{RE}}{\partial \phi_o} = 0, \qquad \frac{\partial S_{RE}}{\partial \alpha} = 0, \qquad \frac{\partial S_{RE}}{\partial p} = 0.$$

This leads to a system of non-linear equations

$$\phi_o = \sum_{i=1}^{n_g} w_i \phi_i - \alpha \sum_{i=1}^{n_g} w_i h_i^p,$$

$$\alpha = \frac{\sum_{i=1}^{n_g} w_i \phi_i h_i^p - \left(\sum_{i=1}^{n_g} w_i \phi_i\right)\left(\sum_{i=1}^{n_g} w_i h_i^p\right)}{\sum_{i=1}^{n_g} w_i h_i^{2p} - \left(\sum_{i=1}^{n_g} w_i h_i^p\right)\left(\sum_{i=1}^{n_g} w_i h_i^p\right)},$$

$$\sum_{i=1}^{n_g} w_i \phi_i h_i^p \log(h_i) - \phi_o \sum_{i=1}^{n_g} w_i h_i^p \log(h_i) - \alpha \sum_{i=1}^{n_g} w_i h_i^{2p} \log(h_i) = 0$$

that has a standard deviation given by

$$\sigma_{RE} = \sqrt{\frac{\sum_{i=1}^{n_g} nw_i (\phi_i - (\phi_o + \alpha h_i^p))^2}{(n_g - 3)}}.$$

B.3. Single term expansion with first-order term

ϕ_o and α are determined from the minimum of the function

$$S_1(\phi_o, \alpha) = \sqrt{\sum_{i=1}^{n_g} w_i \left(\phi_i - (\phi_o + \alpha h_i)\right)^2}$$

that is obtained from

$$\frac{\partial S_1}{\partial \phi_o} = 0, \qquad \frac{\partial S_1}{\partial \alpha} = 0.$$

This leads to a system of linear equations

$$\begin{bmatrix} 1 & \sum_{i=1}^{n_g} w_i h_i \\ \sum_{i=1}^{n_g} w_i h_i & \sum_{i=1}^{n_g} w_i h_i^2 \end{bmatrix} \begin{bmatrix} \phi_o \\ \alpha \end{bmatrix} = \begin{bmatrix} \sum_{i=1}^{n_g} w_i \phi_i \\ \sum_{i=1}^{n_g} w_i \phi_i h_i \end{bmatrix}$$

that has a standard deviation given by

$$\sigma_1 = \sqrt{\frac{\sum_{i=1}^{n_g} n w_i (\phi_i - (\phi_o + \alpha h_i))^2}{(n_g - 2)}}.$$

B.4. Single term expansion with second-order term

ϕ_o and α are determined from the minimum of the function

$$S_2(\phi_o, \alpha) = \sqrt{\sum_{i=1}^{n_g} w_i \left(\phi_i - \left(\phi_o + \alpha h_i^2\right)\right)^2}$$

that is obtained from

$$\frac{\partial S_2}{\partial \phi_o} = 0, \qquad \frac{\partial S_2}{\partial \alpha} = 0.$$

This leads to a system of linear equations

$$\begin{bmatrix} 1 & \sum_{i=1}^{n_g} w_i h_i^2 \\ \sum_{i=1}^{n_g} w_i h_i^2 & \sum_{i=1}^{n_g} w_i h_i^4 \end{bmatrix} \begin{bmatrix} \phi_o \\ \alpha \end{bmatrix} = \begin{bmatrix} \sum_{i=1}^{n_g} w_i \phi_i \\ \sum_{i=1}^{n_g} w_i \phi_i h_i^2 \end{bmatrix}$$

that has a standard deviation given by

$$\sigma_2 = \sqrt{\frac{\sum_{i=1}^{n_g} n w_i (\phi_i - (\phi_o + \alpha h_i^2))^2}{(n_g - 2)}}.$$

B.5. Two-term expansion with first and second-order terms

ϕ_o, α_1 and α_2 are determined from the minimum of the function

$$S_{12}(\phi_o, \alpha_1, \alpha_2) = \sqrt{\sum_{i=1}^{n_g} w_i \left(\phi_i - \left(\phi_o + \alpha_1 h_i + \alpha_2 h_i^2\right)\right)^2}$$

that is obtained from

$$\frac{\partial S_{12}}{\partial \phi_o} = 0, \qquad \frac{\partial S_{12}}{\partial \alpha_1} = 0, \qquad \frac{\partial S_{12}}{\partial \alpha_2} = 0.$$

This leads to a system of linear equations

$$\begin{bmatrix} 1 & \sum_{i=1}^{n_g} w_i h_i & \sum_{i=1}^{n_g} w_i h_i^2 \\ \sum_{i=1}^{n_g} w_i h_i & \sum_{i=1}^{n_g} w_i h_i^2 & \sum_{i=1}^{n_g} w_i h_i^3 \\ \sum_{i=1}^{n_g} w_i h_i^2 & \sum_{i=1}^{n_g} w_i h_i^3 & \sum_{i=1}^{n_g} w_i h_i^4 \end{bmatrix} \begin{bmatrix} \phi_o \\ \alpha_1 \\ \alpha_2 \end{bmatrix} = \begin{bmatrix} \sum_{i=1}^{n_g} w_i \phi_i \\ \sum_{i=1}^{n_g} w_i \phi_i h_i \\ \sum_{i=1}^{n_g} w_i \phi_i h_i^2 \end{bmatrix}$$

that has a standard deviation given by

$$\sigma_{12} = \sqrt{\frac{\sum_{i=1}^{n_g} n w_i (\phi_i - (\phi_o + \alpha_1 h_i + \alpha_2 h_i^2))^2}{(n_g - 3)}}.$$

Appendix C. Calculation details

C.1. 2-D manufactured solutions

The manufactured solutions (MS's) mimic a near-wall turbulent flow [18] at a Reynolds number based on the velocity at the top boundary U_1 and on the domain length L of $Rn = 10^7$. The computational domain is a rectangle with $0.1 \leqslant x \leqslant 1$ and $0 \leqslant y \leqslant 0.25$, where x and y are dimensionless coordinates.

For each MS, we have generated three sets of 21 geometrically similar Cartesian grids. All grids have equally-space nodes along the horizontal x direction and one-sided stretching functions [19] are applied in the vertical y direction to obtain clustered grid nodes near the "wall" ($y = 0$). The three grid sets differ only in the stretching parameter applied at $y = 0$. Grid set A has the smallest near-wall spacing and set C the largest.

Selected boundary conditions are typical of a flat plate boundary-layer flow: specified velocity components at the inlet and at the bottom; specified horizontal velocity component u_x and pressure coefficient C_p at the top boundary and specified C_p pressure coefficient at the outlet. Pressure derivatives at the inlet and bottom are zero (satisfied by the MS's) and velocity derivatives at the outlet are obtained from the MS's.

The calculations of the three MS's were carried out with the finite-difference 2D-flow version of PARNASSOS [20] using the manufactured eddy-viscosity field. PARNASSOS is formally second-order accurate, but first-order velocity derivatives (convection and continuity) and pressure derivatives are approximated with third-order schemes. All calculations were performed with 15 digits precision and the iterative error was reduced to machine accuracy.

C.2. Flow over a flat plate

The statistically-steady flow over a flat plate is assumed to be two-dimensional and incompressible. The computational domain is a rectangle with a length of $1.5L$ and a width of $0.25L$, where L stands for the length of the plate. The inlet boundary is located $0.25L$ upstream of the leading edge of the plate and the outlet boundary $0.25L$ downstream of the trailing edge.

The Reynolds number is defined by $Re_L = \frac{U_\infty L}{\nu}$, where U_∞ is the undisturbed velocity, L is the length of the plate and ν is the kinematic viscosity of the fluid. In this study, we have made calculations for three Reynolds numbers: 10^7, 10^8, and 10^9.

For each Reynolds number, we have generated three sets of 13 geometrically similar Cartesian grids. For $Re_L = 10^7$ and $Re_L = 10^8$, the finest grids include 1537×193 grid nodes and the coarsest 193×25, covering a grid refinement ratio of 8. For $Re_L = 10^9$ the number of grid nodes in the vertical y direction is increased leading to grids having between 1537×225 and 193×29 nodes. Each set contains 3 grids between each doubling of the grid spacing, i.e. there are three groups of 5 grids, each covering a grid refinement ratio of 2.

The grid node distribution in the longitudinal (x) direction (equal for all the sets) is non-uniform with clustering of nodes near the leading and trailing edge of the plate using Vinokur's one or two-sided stretching functions [19]. In all the grids, 2/3 of the nodes in the longitudinal direction are located on the plate; 1/6 are located upstream of the plate and 1/6 downstream of the plate. In the normal (y) direction, one-sided stretching functions are applied to cluster grid nodes close to plate. As for the previous test case, the three sets have different near-wall grid line distances. All the grids of set A have $(y_2^+)_{\max} < 1$, whereas all the grids of set C have $(y_2^+)_{\max} > 1$.

Undisturbed velocity is imposed at the inlet, undisturbed pressure coefficient is imposed at the top boundary and zero streamwise derivatives are assumed at the outlet. On the two segments of the bottom boundary coinciding with the symmetry line we impose $u_y = 0$. u_x and C_p are computed from the momentum equations in the x and y directions, imposing the symmetry conditions at virtual grid nodes.

Boundary conditions for the Spalart and Allmaras (SPAL) one-equation model [23] and the Shear-Stress Transport (SST) $k-\omega$ two-equation model [24] eddy-viscosity models are: at the inlet boundary, the turbulence quantities are constant and

defined from given values of the eddy-viscosity, ν_t, and ω ($(\nu_t)_{inlet} = 0.01\nu$ and $(\omega)_{inlet} = \frac{10U_\infty}{L}$); derivatives of all turbulence quantities with respect to y are set equal to zero at the top boundary; on the two segments of the bottom boundary coinciding with the symmetry line, symmetry conditions ($\partial/\partial y = 0$) are applied directly to the turbulence quantities; on the plate surface, all turbulence quantities are set equal to zero with the exception of ω (that goes to infinity), which is specified at the first grid node away from the wall [25] using the near-wall solution of ω [26]; at the outlet boundary, all streamwise derivatives of the turbulence quantities are assumed to be zero.

As for the previous case, calculations were performed with the finite-difference 2D-flow version of PARNASSOS [20] with 15 digits precision and the iterative error was reduced to machine accuracy.

C.3. Flow over a backward facing step

The flow over a backward facing step has been calculated in a computational domain bounded by two walls and two x constant planes, $-4H$ upstream and $40H$ downstream of the step, where H is the step height. The Reynolds number based on the step height and the velocity of the incoming flow, U_{ref}, is 5×10^5.

All the required flow quantities are specified at the inlet, with the exception of the pressure coefficient, which is extrapolated from the interior of the domain assuming that its second derivative in the streamwise direction is zero. At the walls, the no-slip and impermeability conditions are applied, which leads to $u_x = u_y = 0$. $\tilde{\nu}$ and k are set equal to 0 and ω is specified in the way described above for the flat plate flow [25]. The momentum equation in the normal direction is solved at the wall to obtain the pressure value. At the outlet boundary, u_x, u_y and the turbulence quantities are linearly extrapolated from the interior of the domain. The pressure coefficient is set to zero.

There are two sets of 19 single-block, structured, geometrically similar grids, with coarsest grids of 41×41 nodes and finest grids of 401×401 nodes covering a grid refinement ratio of 10.

As for the previous examples, all the calculations were carried out with the finite-difference, 2D-flow version of PARNASSOS [20] using 15-digits precision and reducing the iterative error to machine accuracy.

C.4. Flow around a tanker

The flow around the KVLCC2 tanker at model scale Reynolds number (4.6×10^6) has been calculated in a computational domain of cylindrical shape. The boundaries of the domain are two $x = constant$ planes at the inlet and outlet, the planes $y = 0$ (symmetry plane of the ship) and $z = 0$ (still water plane), the surface of the ship and a cylindrical surface (external boundary) with the axis along the x direction at the intersection of the symmetry plane of the ship and the still water plane. The inlet and outlet planes are located one ship length (L_{PP}) upstream and downstream of the forward and aft perpendiculars, respectively. The radius of the external boundary is equal to L_{PP}.

We have generated four sets (A, B, C and D) of six nearly geometrically similar grids (using exactly the same settings in the grid generators for each family of grids) in the computational domain described above. All the grids are single-block H–O grids that differ essentially in the streamwise and girthwise node distributions. Although the grids do not respect exact geometric similarity (especially at the bow and stern contours), h_i/h_1 is again defined by Eq. (22). The coarsest grids have 0.7 to 0.8 million cells and the finest 5.3 to 6.1 million cells, covering always a grid refinement ratio of 2.

The following boundary conditions are applied at the boundaries of the computational domain: velocity components specified from a potential flow solution and pressure extrapolated from the interior of the domain at the inlet; the eddy-viscosity is set equal to 0.01 of the kinematic viscosity, $\nu_t = 0.01\nu$ and the non-dimensional value of ω is set equal to 10, $\omega = 10U_\infty/L_{PP}$. At the outlet, zero streamwise derivatives are assumed for all flow variables. At the symmetry plane of the ship, the normal velocity component is set equal to zero. Tangential velocity components and pressure are obtained from the solution of the momentum equations with the symmetry conditions applied at virtual nodes, when the symmetry plane of the ship coincides with the bottom of the computational domain (extreme of the normal grid lines). Otherwise, the symmetry conditions are applied directly to the tangential velocity components and to the pressure. Symmetry conditions are applied directly to k and ω. At the still water plane (no gravity waves), girthwise velocity is set equal to zero and tangential velocity components and pressure are obtained from the solution of the continuity, streamwise and normal momentum equations with the symmetry conditions applied at virtual nodes. Girthwise derivatives are set equal to zero for k and ω. Tangential velocity components and pressure are imposed from a potential flow calculation at the external boundary. Normal derivatives of k and ω are assumed to be zero. No-slip condition applied directly at the wall, i.e. velocity components set equal to zero and wall shear-stress computed from the normal velocity derivative at the ship surface. Normal pressure derivative and k are set equal to zero. As in the previous test cases, ω is specified at the first grid node away from the wall [25]. It is noted that the maximum y_2^+ of all 24 grids is below 0.8.

The calculations were made with the three-dimensional version of PARNASSOS [30,31] using the SST $k-\omega$ two-equation eddy-viscosity turbulence model [24]. We have used 15 digits precision, but we have not converged all solutions to machine accuracy. Nevertheless, we have ensured that the iterative error was reduced to at least three orders of magnitude below the discretization error [12].

References

[1] P.J. Roache, Verification and Validation in Computational Science and Engineering, Hermosa Publishers, Albuquerque, New Mexico, 1998.
[2] P.J. Roache, Fundamentals of Verification and Validation, Hermosa Publishers, Albuquerque, New Mexico, 2009.
[3] ASME Committee PTC 61: ANSI Standard V&V 20: Guide on Verification and Validation in Computational Fluid Dynamics and Heat Transfer, 2009.
[4] I.B. Celik, U. Ghia, P.J. Roache, C.J. Freitas, H. Coleman, P.E. Raad, Procedure for estimation and reporting of uncertainty due to discretization in CFD applications, J. Fluids Eng. 130 (July 2008).
[5] C.J. Roy, Review of code and solution verification procedures for computational simulation, J. Comput. Phys. 205 (1) (May 2005) 131–156.
[6] F. Stern, R.V. Wilson, H. Coleman, E. Patterson, Comprehensive approach to verification and validation of CFD simulations—Part 1: Methodology and procedures, J. Fluids Eng. 123 (4) (December 2001) 793–802.
[7] T. Xing, F. Stern, Factors of safety for Richardson extrapolation, J. Fluids Eng. 132 (6) (June 2010), 061403, 13 pp.
[8] Ismail Celik, Ertan Karaismail, Francisco Elizalde Blancas, Don Parsons, Hayri Sezer, Error estimation using hybrid methods, in: ASME 2012 Fluids Engineering Division Summer Meeting, 2012, pp. 1621–1642, Paper No. FEDSM2012-72290.
[9] L. Eça, M. Hoekstra, P.J. Roache, Verification of calculations: an overview of the Lisbon workshop, in: AIAA Computational Fluid Dynamics Conference, Toronto, June 2005, AIAA Paper 4728.
[10] L. Eça, M. Hoekstra, P.J. Roache, Verification of calculations: an overview of the 2nd Lisbon workshop, in: AIAA Computational Fluid Dynamics Conference, Miami, June 2007, AIAA Paper 4089.
[11] L. Eça, M. Hoekstra, P.J. Roache, H.C. Coleman, Code verification, solution verification and validation: an overview of the 3rd Lisbon workshop, in: AIAA Computational Fluid Dynamics Conference, San Antonio, June 2009, AIAA Paper 3647.
[12] L. Eça, M. Hoekstra, Evaluation of numerical error estimation based on grid refinement studies with the method of the manufactured solutions, Comput. Fluids 38 (8) (September 2009) 1580–1591.
[13] L. Eça, M. Hoekstra, An evaluation of verification procedures for CFD applications, in: 24th Symposium on Naval Hydrodynamics, Fukuoka, Japan, July 2002.
[14] L. Eça, M. Hoekstra, Error estimation based on grid refinement studies: a challenge for grid generation, in: Conferência de Métodos Numéricos en Ingineria 2009, SEMNI Barcelona, Spain, July 2009.
[15] J.O. Rawlings, S.G. Pantula, D.A. Dickey, Applied Regression Analysis: A Research Tool, 2nd ed., Springer, New York, 1998.
[16] L. Eça, M. Hoekstra, Discretization uncertainty estimation based on a least-squares version of the Grid Convergence Index, in: 2nd Workshop on CFD Uncertainty Analysis, Instituto Superior Técnico, Lisbon, October 2006.
[17] L. Eça, M. Hoekstra, Testing uncertainty estimation and validation procedures in the flow around a backward facing step, in: 3rd Workshop on CFD Uncertainty Analysis, Instituto Superior Técnico, Lisbon, October 2008.
[18] L. Eça, M. Hoekstra, G. Vaz, Manufactured solutions for steady-flow Reynolds-averaged Navier–Stokes solvers, Int. J. Comput. Fluid Dyn. 26 (5) (2012) 313–332.
[19] M. Vinokur, On one-dimensional stretching functions for finite-difference calculations, J. Comput. Phys. 50 (1983) 215–234.
[20] José M.Q.B. Jacob, L. Eça, 2-D incompressible steady flow calculations with a fully coupled method, in: VI Congresso Nacional de Mecânica Aplicada e Computacional, Aveiro, April 2000.
[21] L. Eça, M. Hoekstra, The numerical friction line, J. Mar. Sci. Technol. 13 (4) (2008) 328–345.
[22] L. Eça, M. Hoekstra, Code verification and verification of calculations with RANS solvers, in: AVT-147—Computational Uncertainty in Military Vehicle Design, Athens, December 2007.
[23] P.R. Spalart, S.R. Allmaras, A one-equation turbulence model for aerodynamic flows, in: AIAA 30th Aerospace Sciences Meeting, Reno, January 1992.
[24] F.R. Menter, Two-equation eddy-viscosity turbulence models for engineering applications, AIAA J. 32 (August 1994) 1598–1605.
[25] L. Eça, M. Hoekstra, On the grid sensitivity of the wall boundary condition of the $k-\omega$ model, J. Fluids Eng. 126 (6) (November 2004) 900–910.
[26] D.C. Wilcox, Turbulence Modeling for CFD, 2nd ed., DCW Industries, 1998.
[27] L. Larsson, F. Stern, V. Bertram (Eds.), Gothenburg 2000—A Workshop on Numerical Ship Hydrodynamics, September 2000.
[28] T. Hino (Ed.), CFD Workshop Tokyo 2005, March 2005.
[29] L. Larsson, F. Stern, M. Visonneau (Eds.), Gothenburg 2010—A Workshop on Numerical Ship Hydrodynamics, December 2010.
[30] A. van der Ploeg, L. Eça, M. Hoekstra, Combining accuracy and efficiency with robustness in ship stern flow computations, in: 23rd Symposium on Naval Hydrodynamics, Val de Reuil, France, 2000.
[31] M. Hoekstra, Numerical simulation of ship stern flows with a space-marching Navier–Stokes method, PhD Thesis, Delft, Netherlands, 1999.